Geochemical, age, and isotopic constraints on the location of the Sino–Korean/Yangtze Suture and evolution of the Northern Dabie Complex, east central China

Derek L. Bryant
John C. Ayers†
Department of Earth and Environmental Sciences, Vanderbilt University, Nashville, Tennessee 37235, USA

Shan Gao
Faculty of Earth Sciences, China University of Geosciences, Wuhan 430074, China, and *Key Laboratory of Continental Dynamics, Department of Geology, Northwest University, Xi'an 710069, China*

Calvin F. Miller
Department of Earth and Environmental Sciences, Vanderbilt University, Nashville, Tennessee 37235, USA

Hongfei Zhang
Faculty of Earth Sciences, China University of Geosciences, Wuhan 430074, China

ABSTRACT

The Northern Dabie Complex in east central China lies between the Sino–Korean plate to the north and the Yangtze plate to the south. The Northern Dabie Complex has been variously proposed to represent a Paleozoic magmatic arc on the Sino–Korean plate, an exhumed piece of subducted Yangtze plate crust, or crust produced almost entirely by Cretaceous extension-related magmatism. Trace element compositions of Northern Dabie Complex orthogneisses and granites show arc signatures similar to those of ultra-high-pressure rocks in the central Dabie, but no mineralogical evidence of ultra-high-pressure metamorphism is present in the samples investigated here. Field relationships, textures, major and trace element compositions, and ion microprobe U-Pb zircon protolith crystallization ages reveal three distinct types of gneiss: diorite gneiss xenoliths (770 ± 26 Ma, 95% confidence limit), those within first-genation highly deformed migmatitic grey gneisses (747 ± 14 Ma), and those cross-cut by second-generation Cretaceous weakly foliated felsic gneisses (127 ± 4 Ma). Unfoliated Cretaceous granites (117 ± 11 Ma, monazite Th-Pb age = 117 ± 1 Ma) intrude second-generation gneisses. Cretaceous second-generation gneisses and granites yield zircon inheritance ages of ca. 2 Ga, 700–800 Ma, and (rarely) 227–271 Ma, indicating that the Northern Dabie Complex is not simply a Cretaceous extensional terrane. The 700–800 Ma zircon ages are similar to those of granitic gneisses from the central ultra-high-pressure zone (698 ± 47 Ma) and are characteristic of the Yangtze craton. ε_{Nd} values suggest that Cretaceous rocks in the Northern Dabie Complex formed by partial melting of basement with very low ε_{Nd} and not by melting of first-generation or diorite gneisses. Nd-depleted mantle model ages are consistent with the time of formation of the Yangtze craton at 1.4–2.5 Ga. The Northern Dabie Complex is interpreted to be an extension of the Yangtze craton that was unaffected by ultra-high-pressure metamorphism. The Sino–Korean/Yangtze suture must lie to the north of the Northern Dabie Complex.

Keywords: metamorphism, monazite, zircon, geochronology, Dabie Mountains, ion probe dating.

INTRODUCTION

China's Dabie-Sulu orogen, the most extensive ultra-high-pressure belt in the world, resulted from a collision between the Sino–Korean and Yangtze lithospheric plates in the Triassic (e.g., Hacker et al., 2000; Ayers et al., 2002). This collision resulted in the subduction of Yangtze continental crust beneath the Sino–Korean plate as evidenced by the formation of ultra-high-pressure mineral assemblages preserved in crustal rocks of the central Dabie ultra-high-pressure zone (Fig. 1). Ultra-high-pressure index minerals such as coesite, jadeite, and diamond found in isolated pods in the central Dabie Mountains (Xu et al., 1992) suggest that portions of the Yangtze craton subducted to depths ≥125 km. Detachment of dense eclogitic oceanic crust may have triggered exhumation of the buoyant continental crust ''diachronously between 240 and ~225–210 Ma'' (Hacker et al., 2000).

Currently the Northern Dabie Complex lies between the Sino–Korean and Yangtze plates, but its plate assignment is uncertain. Because proposed locations of the suture between the Sino–Korean and Yangtze plates remain controversial, the position of the Northern Dabie Complex before and during the collision is uncertain (Fig. 1). Prevailing hypotheses (Fig. 2) are that the Northern Dabie Complex (1) was part of the hanging wall of the Sino–Korean continental plate and contains a Paleozoic magmatic arc complex (Zhai et al., 1994); (2) was part of the partially subducted Yangtze continental plate that experienced ultra-high-pressure metamorphism (Tsai and Liou, 2000); and (3) is almost entirely the result of post-collisional extensional magmatism in the Cretaceous (Hacker et al., 1998). This study

†Corresponding author e-mail: john.c.ayers@vanderbilt.edu.

GSA Bulletin; May/June 2004; v. 116; no. 5/6; p. 698–717; doi: 10.1130/B25302.1; 10 figures; 7 tables.

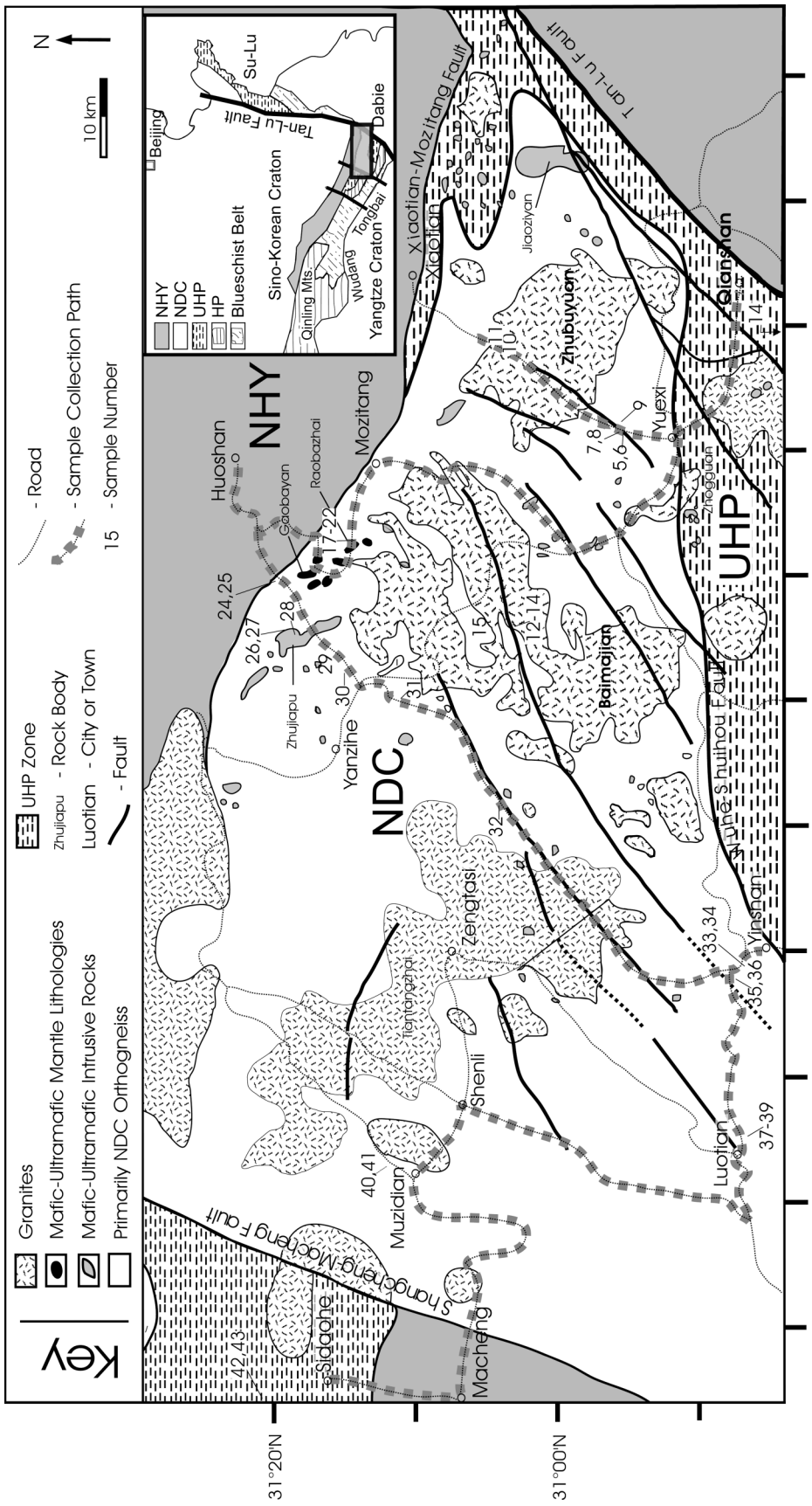

Figure 1. Generalized geologic map of Northern Dabie Complex (after Zhang et al., 1996, 2002; and Nelles Verlag, 1998). Sample numbers correspond to sample names given in Table 1. HP—high pressure, UHP—ultra-high-pressure, NDC—Northern Dabie Complex, NHY—North Huaiyang.

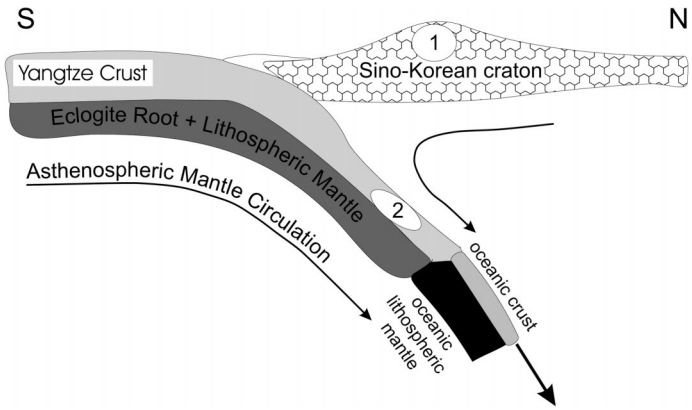

Figure 2. Schematic cross section showing collision of Yangtze and Sino–Korean plates during Triassic (after Liou et al., 1998). Northern Dabie Complex is represented by area 1 according to magmatic arc hypothesis (Zhai et al., 1994) and by area 2 according to ultra-high-pressure metamorphism hypothesis (Tsai and Liou, 2000). According to extensional magmatism hypothesis, the Northern Dabie Complex did not exist during collision (Hacker et al., 1998).

tests these competing hypotheses using representative samples collected throughout the Northern Dabie Complex. Ion microprobe zircon U-Pb and monazite Th-Pb ages are used to establish the magmatic ages of protoliths and from inherited grains the ages of source rocks, which can be used to locate the suture because the basement rocks of the northern Yangtze and southern Sino–Korean cratons have distinctly different ages (700–800 and 400–480 Ma, respectively, see Hacker et al., 1998). Sm-Nd isotopic data are used to calculate depleted mantle model ages to test whether the crust in the Northern Dabie Complex is Cretaceous (hypothesis #3), Paleozoic (hypothesis #1), or older. Trace element systematics are used to constrain the tectonic setting in which the rocks formed, for example, volcanic arc (hypothesis #1) or extension/rifting (hypothesis #3).

Geologic Setting

The Dabie Mountains consist of four distinct tectonic zones. From north to south, these are (1) the North Huaiyang, (2) the Northern Dabie Complex, (3) the ultra-high-pressure, and (4) the high-pressure zones. The North Huaiyang contains greenschist facies volcanic and sedimentary rocks (Hacker et al., 1996). The ultra-high-pressure is the only zone of the four to contain widespread evidence of ultra-high-pressure metamorphism and consists primarily of gneiss containing pods of ultra-high-pressure eclogite, garnet peridotite, jadeite quartzite, and marble. The high-pressure zone is mainly muscovite-albite and quartzofeldspathic two-mica gneisses with minor eclogite, amphibolite, marble, blueschist, and metaphosphorites (Zhang et al., 2002).

The focus of this study, the Northern Dabie Complex, is bounded by five faults or shear zones (Fig. 1). To the north it is bounded by the Xiaotian–Mozitang fault, to the southeast by the Wuhe–Shuihou fault (Zhang et al., 2002), to the southwest by the Wumiao–Taihu fault (not shown in Fig. 1), to the east by the Tan–Lu fault or a fault contact between the ultra-high-pressure and Northern Dabie Complex, and to the west by the Shangcheng-Macheng fault (Ratschbacher et al., 2000). Granite intrusions make up ~50% of the area of the Northern Dabie Complex. They intrude several generations of abundant orthogneiss. Minor metasedimentary rocks consist of marble, quartzite, calc-silicates, biotite schist, and banded iron formations (Wang et al., 1996). Rare mafic/ultramafic rocks occur as lenses along the northern and southern borders of the Northern Dabie Complex and consist of amphibolites, peridotites, mafic granulites, and retrogressed eclogites. Several localities in the northernmost Northern Dabie Complex just south of the Xiaotian-Mozitang fault have yielded evidence of ultra-high-pressure metamorphism, starting with the discovery of supersilicic omphacite (P >2.5 GPa) in the Raobazhai eclogite body (Tsai and Liou, 2000). The eclogites yielded Triassic Sm-Nd mineral-whole rock isochron ages consistent with the timing of continental subduction (Li et al., 1993). More recently microdiamonds have been found in eclogites from Baizhangya and Huangweihe (Xu et al., 2003). If the entire Northern Dabie Complex experienced ultra-high-pressure metamorphism, we would expect to find abundant Triassic zircon U-Pb ages such as found in the central Dabie ultra-high-pressure zone (Ayers et al., 2002; Hacker et al., 2000).

SAMPLES

Sample Descriptions

Samples of all major nonsedimentary Northern Dabie Complex lithologies were collected, with an emphasis on gneisses, and several samples of ultra-high-pressure zone gneisses were also collected for comparison (Fig. 1, Table 1). Each sample consisted of ~5–20 kg of rock, most of which we divided for thin sections, powdering for geochemistry (± Sm-Nd isotopic analysis), and—for selected samples—mineral separation for geochronology. The samples consist of five general types of rocks: Northern Dabie Complex gneisses, Northern Dabie Complex granites, mafic/ultramafic rocks from the Northern Dabie Complex, ultra-high-pressure zone gneisses, and various metasedimentary rocks of the Northern Dabie Complex and North Huaiyang (see Zhang et al., 1996, for details). Although not reported here, we have observed and others have reported the presence of granulites from several localities within the central Northern Dabie Complex (Zhang et al., 1996; Zheng et al., 2001).

Field relationships show that the Northern Dabie Complex contains several generations of visually distinctive gneisses. The first-genation gneisses are gray-colored, locally migmatitic granodioritic orthogneisses with foliation that is often nonplanar and sometimes complexly folded (Fig. 3, A and C). They contain 35–70% plagioclase feldspar, 5–35% quartz, 5–25% K-feldspar, 1–10% biotite, 0–10% hornblende, and accessory opaque minerals, apatite, sphene, garnet, zircon, and chlorite. These gneisses are sometimes crosscut by second-generation orthogneisses that are often lighter in color than the first-genation and have planar foliation (Fig. 3B). Except QLB-3, the second-generation gneisses consist of ~60% plagioclase feldspar, 15–30% K-feldspar, 5–15% quartz, 2–20% hornblende, 1–15% biotite, and accessory opaque minerals, apatite, sphene, zircon, and chlorite. A third, less common, dark gray dioritic gneiss is often massive or displays subtle foliation or migmatization and veining and occurs as xenoliths within and cross cut by both first- and second-generation gneisses (Fig. 3A). It consists of 50–65% plagioclase feldspar, 10–15% K-feldspar, 10–20% hornblende, 7–15% biotite, and accessory opaque minerals, quartz, apatite, sphene, epidote, zircon, and chlorite.

The second-generation gneiss is often in

TABLE 1. SUMMARY OF SAMPLES COLLECTED

Sample	Collection order no.	Locality	Latitude (N)	Longitude (E)	Geochem.	Dating*
NDC Granite						
BMJ-1	12	Baojia	31°02.928′	116°06.876′	√	M,Z
BMJ-2	13	Baojia	~31°02.928′	~116°06.876′		
BMJ-4	15	Baojia	31°05.252′	116°06.486′	√	
ZB-1	10	Zhubuyuan	31°03.365′	116°28.107′	√	
ZB-2	11	Zhubuyuan	31°04.017′	116°29.124′		
2nd Gen. NDC Gneiss						
BMJ-3	14	Baojia	~31°02.928′	~116°06.876′	√	Z (NM)
DSC-1	30	Daoshicong	31°14.945′	116°02.058′	√	
LTS-2	25	Lutushishan	31°21.041′	116°10.382′	√	
MJC-1	29	Mianjiangchong	31°16.083′	116°02.564′	√	
QLB-3	39	Qilibai	30°46.675′	115°25.352′	√	Z (NM)
WW-1	5	Wangwu	30°55.194′	116°21.528′	√	
WW-2	6	Wangwu	30°55.194′	116°21.528′	√	
WW-4	8	Wangwu	30°55.234′	116°21.651′	√	Z (NM)
WW-5	9	Wangwu	30°55.298′	116°22.182′		
ZJP-3	28	Zhujiapu	31°18.331′	116°05.120′		
1st Generation NDC Gneiss						
FUZL-1	35	Fuzhiling	30°47.299′	115°37.968′	√	
LJW-1	32	Loujiawan	31°04.138′	115°51.535′	√	
LTS-1	24	Lutushishan	31°21.041′	116°10.382′	√	Z (NM)
MSH-1	31	Manshuihe	31°11.166′	116°00.200′	√	
QLB-2	38	Qilibai	30°46.675′	115°25.352′	√	Z (NM)
RBZ-14	22	Raobazhai	31°15.810′	116°13.254′	√	
WW-3	7	Wangwu	30°55.234′	116°21.651′	√	Z (NM)
YZS-2	34	Yazhangshu	30°46.902′	115°38.859′	√	
Diorite Gneiss						
FUZL-2	36	Fuzhiling	30°47.299′	115°37.968′	√	
QLB-1	37	Qilibai	30°46.675′	115°25.352′	√	Z (NM)
YZS-1	33	Yazhangshu	30°46.902′	115°38.859′	√	
NDC Mafic/Ultra-mafics						
DB-117	40	Muzhidian	31°12.607′	115°22.602′	√	(NM, NZ)
RBZ-1	17	Raobazhai	31°15.810′	116°13.254′	√	(NM, NZ)
RBZ-2	18	Raobazhai	31°15.810′	116°13.254′	√	
RBZ-3	19	Raobazhai	31°15.810′	116°13.254′	√	
RBZ-4	20	Raobazhai	31°15.810′	116°13.254′	√	
RBZ-5-13	21	Raobazhai	31°15.810′	116°13.254′		
YRZ-2	3	Yerenzhai	30°40.108′	116°29.114′		
ZJP-1	26	Zhujiapu	31°19.454′	116°06.642′		
ZJP-2	27	Zhujiapu	31°19.454′	116°06.642′		
UHP Zone Gneiss						
SDH-1	42	Sidaohe	31°20.810′	115°03.529′	√	
YRZ-3	4	Yerenzhai	30°40.108′	116°29.114′	√	
UHP Zone Granitic Gneiss						
SDH-2	43	Sidaohe	31°20.810′	115°03.529′		
SZS-1	1	Sanzushi	30°40.408′	116°29.877′	√	Z† (NM)
YRZ-1	2	Yerenzhai	30°40.108′	116°29.114′	√	Z‡

Note: NDC—Northern Dabie Complex; UHP—Ultra-high-pressure.
*Indicates geochronologic analysis on either monazite (M) or zircon (Z) separates. "NM" and "NZ" indicate that the sample was separated and monazite or zircon was not found.
†Zircon separates taken from sample provided by Hongfei Zhang.
‡Zircon separates provided by Hongfei Zhang.

contact with the Northern Dabie Complex granites, which show no foliation in outcrop or hand samples (Fig. 3C). The granites studied in this project, the Zhuboyuan and Baimajian, have subequal amounts of plagioclase feldspar, K-feldspar, and quartz, with ~5–10% biotite but no hornblende, but they are distinctive in the field. The Zhuboyuan granite is medium- to coarse-grained with abundant pink K-feldspar, whereas the Baimajian is finer-grained with less K-feldspar.

Mafic and ultramafic rocks of the Northern Dabie Complex represent a wide range of rock types including retrogressed eclogites, peridotites, pyroxenites, granulites, and gabbros. Mantle lithologies including eclogites and peridotites are rare, occurring exclusively in the northernmost Northern Dabie Complex just south of the Xiaotian–Mozitang fault (Fig. 1) as meter-scale bodies. These samples include retrogressed eclogites and peridotites from the Raobazhai mafic/ultramafic body (Zhai et al. (1994); Wang et al. (1996); Tsai and Liou (2000)) and microdiamond-bearing lenses of granulite-facies–overprinted eclogite enclosed in gneiss (Baizhangya) or garnet peridotite (Huangweihe) as described by Xu et al. (2003). It is now accepted that ultra-high-pressure minerals are preserved only in mafic lithologies in the central Dabie, and that the felsic gneisses that host them also experienced ultra-high-pressure M (metamorphism) but were completely retrogressed (Liou et al., 1998). The same may be true for the ultra-high-pressure mafic bodies and their host rocks in the northernmost Northern Dabie Complex. However, Suo et al. (2003) report that the eclogites in the northernmost Northern Dabie Complex are always separated from adjacent gneisses by faults. Likewise, Tsai and Liou (2000) observed the Rhaobazhai mafic body to be fault-bounded. The relationship between the mafic bodies and adjacent gneisses in the Northern Dabie Complex therefore remains unclear. Post-collisional mafic/ultramafic intrusive rocks including the Zhujiapu and Jiaoziyan gabbros (Fig. 1) are more widely distributed in the Northern Dabie Complex, yield Cretaceous ages, and are relatively undeformed (Jahn et al., 1999). Zhang et al. (1996) report the occurrence in five localities of granulites that occur as lenses, blocks, or layers in amphibolites or gneisses. The granulites are located mostly in the western Northern Dabie Complex but span the north-south breadth and were interpreted to have formed in situ at ~800–830 °C and 10–14 kbar.

Two different varieties of ultra-high-pressure zone gneisses were also collected to compare with Northern Dabie Complex gneisses and granites. The first is "ultra-high-pressure zone common gneiss," dark gray with millimeter-sized garnets and strong nonplanar foliation. The second is "ultra-high-pressure zone granitic gneiss," which is lighter in color than the common gneiss and has a weak planar foliation. The ultra-high-pressure zone granitic gneisses, previously referred to as "foliated garnet-bearing granites" by H. Zhang et al. (2001), also contain coarse-grained garnets. These occur in some outcrops as clusters centered in a leucocratic ring where the aligned biotite present throughout the rest of the rock is absent.

METHODS

A detailed description of sample preparations, analysis parameters, and standard, replicate, and blank analyses is provided in Bryant (2002).

Whole-Rock Chemistry

Whole-rock geochemical analysis was performed at Northwest University, Xi'an, China. Major element analysis of glass disks was carried out using a Rigaku RIX 2100 X-ray fluorescence (XRF) spectrometer at 50-mA beam current and 50-kV acceleration voltage. Trace elements were analyzed in solution using a Perkin-Elmer Elan 6100 DRC ICP-MS.

TABLE 2. CHEMICAL COMPOSITIONS OF SELECTED SAMPLES

Rock type	NDC Granite			2nd Generation NDC Gneiss								1st Generation NDC Gneiss							
Sample	BMJ-1	BMJ-4	ZB-1	BMJ-3	DSC-1	LTS-2	MJC-1	QLB-3	WW-1	WW-2	WW-4	FUZL-1	LJW-1	LTS-1	MSH-1	QLB-2	RBZ-14	WW-3	YZS-2
SiO_2	73.2	72.6	73.0	63.6	65.0	62.8	57.5	74.5	59.2	59.6	61.8	62.3	68.7	58.6	68.5	59.6	64.9	69.3	65.6
TiO_2	0.21	0.26	0.28	0.69	0.70	0.41	0.80	0.21	0.90	0.83	0.74	0.76	0.66	0.65	0.44	1.13	0.62	0.64	0.55
Al_2O_3	14.2	14.2	14.3	16.4	14.2	19.0	17.5	13.3	17.0	17.0	16.5	17.6	14.1	19.7	16.3	15.6	13.5	14.0	17.4
Fe_2O_3	1.67	1.89	1.91	5.10	6.41	4.03	7.13	1.76	6.73	6.61	5.71	5.57	4.78	5.85	2.56	8.35	5.40	4.90	3.70
MnO	0.03	0.03	0.04	0.08	0.11	0.14	0.10	0.04	0.09	0.09	0.08	0.14	0.12	0.14	0.03	0.15	0.16	0.08	0.07
MgO	0.40	0.42	0.38	1.90	2.60	0.77	3.10	0.34	2.59	2.65	2.40	1.41	1.62	1.51	0.62	2.89	3.16	1.28	1.06
CaO	1.40	1.48	1.22	4.71	4.57	2.57	5.60	1.22	4.92	3.35	4.78	3.78	3.83	4.14	2.04	5.18	6.60	2.74	3.14
Na_2O	3.76	3.69	3.83	4.82	4.13	5.19	4.22	3.55	4.23	4.42	4.48	5.97	4.58	5.51	4.81	4.71	4.19	3.69	5.20
K_2O	4.95	5.11	5.40	2.01	1.58	5.02	3.03	4.91	2.96	3.60	2.47	2.19	1.12	3.72	4.27	1.73	1.71	2.88	2.86
P_2O_5	0.06	0.08	0.08	0.28	0.14	0.17	0.35	0.05	0.37	0.37	0.32	0.24	0.23	0.32	0.15	0.35	0.16	0.20	0.18
L.O.I.	0.50	0.41	0.22	0.58	0.47	0.54	0.48	0.14	0.57	1.62	0.53	0.34	0.39	0.53	0.45	0.57	0.34	0.74	0.90
Total	100.4	100.2	100.7	100.2	99.9	100.6	99.7	99.9	99.5	100.1	99.9	100.3	100.2	100.7	100.1	100.3	100.7	100.5	100.6
Li	30.3	28.1	25.0	19.2	1.98	5.32	13.1	11.3	11.2	18.0	9.84	20.0	7.06	7.87	6.31	19.9	4.13	9.63	18.3
Be	2.92	3.16	3.66	2.18	1.83	1.13	1.93	0.848	1.72	1.67	1.70	4.09	1.68	1.21	1.43	2.02	2.83	1.39	3.43
Sc	2.42	2.68	2.70	9.32	4.09	6.18	17.7	2.84	11.3	12.5	9.04	13.4	16.9	7.66	2.75	15.6	11.8	11.1	6.30
V	14.9	18.5	16.9	87.5	10.2	13.6	132	12.9	114	100	91.8	52.5	94.4	32.2	31.5	146	98.2	57.5	35.1
Cr	5.55	4.51	2.89	12.0	4.09	1.21	26.6	2.41	19.4	18.1	32.0	4.47	7.31	1.78	0.743	7.55	68.1	10.6	3.18
Co	111	141	120	99.1	161	53.1	87.6	146	73.3	71.7	79.2	73.0	107	32.2	123	95.1	125	94.9	59.3
Ni	3.74	3.29	2.37	9.54	3.26	2.02	19.5	2.07	14.5	12.6	18.4	4.03	6.99	1.99	1.90	14.0	43.8	7.32	3.83
Cu	3.50	3.57	3.49	7.70	2.20	5.79	12.1	2.32	13.0	19.0	8.13	16.5	10.9	10.5	9.78	37.0	20.1	124	23.1
Zn	34.5	37.9	33.4	72.8	11.9	72.0	78.6	36.9	81.8	80.4	68.9	82.5	74.3	90.5	47.6	92.4	86.2	74.0	48.7
Ga	18.8	19.2	19.3	19.8	14.1	20.2	23.5	15.8	21.3	19.2	19.4	26.1	17.2	21.7	22.7	21.0	16.3	17.2	21.4
Rb	163	186	195	59.1	74.0	60.7	63.3	64.9	54.3	88.0	48.8	75.2	25.0	59.5	61.2	42.3	26.6	56.7	118
Sr	278	283	234	782	115	609	937	164	832	598	868	434	355	782	1060	467	226	402	586
Y	14.7	18.2	20.5	21.1	22.8	12.6	30.2	6.64	24.2	24.3	16.3	65.0	32.4	24.2	16.9	31.9	28.0	45.4	33.4
Zr	177	209	220	166	128	603	253	206	194	197	164	432	157	517	261	148	110	213	209
Nb	13.2	15.0	20.8	9.23	9.31	5.68	11.0	3.91	11.8	10.1	8.24	33.1	5.45	15.0	9.91	12.7	11.9	9.30	21.5
Sn	1.39	1.73	1.87	1.93	1.12	0.603	1.66	0.431	1.37	1.34	1.00	4.30	1.49	0.632	1.40	1.89	2.35	2.46	4.13
Cs	2.37	2.76	2.97	1.66	0.538	0.366	1.02	1.59	0.959	1.05	1.16	1.66	0.395	0.487	0.315	2.08	0.197	1.31	2.69
Ba	1330	1240	953	979	1590	4970	2130	942	1930	1950	1700	1060	357	3970	2400	431	618	1560	753
La	65.4	67.4	75.5	27.3	22.6	61.9	45.2	29.3	48.4	34.9	39.8	60.8	23.4	68.5	55.4	22.4	22.9	37.4	27.7
Ce	112	119	131	59.8	44.7	97.2	95.2	54.3	95.9	73.2	75.7	121	49.2	122	101	43.3	45.7	75.6	60.8
Pr	12.0	12.8	14.0	7.81	5.03	10.3	12.1	6.07	11.6	9.37	9.14	13.8	6.30	13.7	11.1	5.53	5.69	9.77	7.29
Nd	38.9	41.2	45.1	32.8	18.2	35.0	49.8	21.2	45.8	37.6	35.8	53.9	27.1	50.5	41.3	25.4	23.0	41.9	27.7
Sm	5.66	6.02	6.73	6.25	3.62	4.62	9.13	3.28	7.91	6.80	5.99	11.0	5.73	7.35	6.33	6.64	4.70	8.79	5.09
Eu	1.01	0.985	1.10	1.97	0.73	3.43	2.20	1.28	2.21	1.94	1.81	2.44	1.60	2.83	1.90	1.62	1.07	2.32	1.33
Gd	4.41	4.77	5.32	4.78	3.15	3.89	7.22	2.65	6.14	5.35	4.71	9.96	5.17	6.16	4.89	5.89	4.15	7.52	4.27
Tb	0.564	0.624	0.706	0.706	0.551	0.466	1.03	0.337	0.853	0.771	0.628	1.65	0.898	0.812	0.603	1.01	0.714	1.26	0.720
Dy	2.80	3.24	3.72	3.85	3.40	2.35	5.53	1.64	4.46	4.15	3.23	9.94	5.40	4.40	3.04	5.85	4.36	7.52	4.48
Ho	0.521	0.641	0.724	0.775	0.779	0.451	1.07	0.294	0.863	0.826	0.595	2.24	1.20	0.876	0.56	1.22	0.975	1.65	1.01
Er	1.33	1.65	1.87	1.95	2.06	1.16	2.60	0.683	2.16	2.10	1.45	5.98	3.01	2.23	1.42	2.85	2.60	4.13	2.79
Tm	0.196	0.252	0.285	0.288	0.335	0.184	0.371	0.097	0.318	0.307	0.207	1.00	0.453	0.323	0.193	0.423	0.416	0.61	0.473
Yb	1.38	1.82	2.06	2.03	2.57	1.38	2.53	0.656	2.24	2.14	1.41	7.81	3.23	2.23	1.24	2.98	3.14	4.29	3.74
Lu	0.209	0.287	0.314	0.311	0.402	0.234	0.375	0.107	0.326	0.316	0.213	1.32	0.493	0.352	0.178	0.482	0.508	0.650	0.570
Hf	6.78	8.03	8.06	5.83	6.48	11.7	7.05	7.45	5.72	5.64	5.18	11.9	5.93	9.93	7.55	5.21	5.23	7.24	5.99
Ta	1.32	1.44	2.02	0.801	0.976	0.284	0.518	0.465	0.743	0.660	0.774	2.27	0.493	0.470	0.550	0.891	1.24	0.905	2.59
Pb	41.5	39.0	38.9	18.9	16.6	22.2	20.7	22.1	17.5	14.7	17.1	18.9	14.6	17.3	28.2	15.7	12.6	17.7	24.8
Th	22.8	25.3	28.8	5.17	7.58	3.31	3.24	5.36	4.83	3.50	5.11	11.2	3.77	1.97	8.59	4.87	3.88	5.15	15.3
U	3.07	4.01	3.42	1.66	1.42	0.473	0.377	1.63	0.639	0.629	0.928	1.75	0.477	0.262	0.252	3.57	3.09	0.645	2.02

Geochronology

Zircon and monazite mineral separates were mounted in epoxy, polished, and examined using backscattered electron and/or cathodoluminescence imaging to reveal internal zoning and core/rim growth relationships. This was done using scanning electron microscopes at Vanderbilt University and the University of California, Los Angeles, and the electron microprobe at the University of Tennessee, Knoxville. We then analyzed spots on individual grains with the Cameca ims 1270 ion microprobe at UCLA using standard procedures outlined in Quidelleur et al. (1997) and Miller et al. (2000). Zircon AS3 (1099.1 ± 0.5 Ma, Paces and Miller, 1993) was used as a standard. The monazite and zircon data were corrected for common lead using a ^{204}Pb correction except for zircons that met two of the following three criteria, in which case a ^{208}Pb correction was used: (1) the sample is <300 Ma, (2) the sample has a low amount of Th, or (3) the ratio ^{208}Pb/^{204}Pb was <400 (see Ayers et al., 2002). Most of the common lead is believed to have been introduced during sample preparation (M. Grove, 2001, personal commun.), so common lead ratios were calculated using the model of Stacey and Kramers (1975) for the present day. We report ^{206}Pb-^{238}U ages (with 95% confidence limits) as best estimates of sample ages because they have smaller errors than ^{207}Pb-^{235}U ages. Isoplot/Ex version 2.49 (Ludwig, 2000) was used to construct concordia and cumulative age probability diagrams.

Sm-Nd Isotopic Composition

Powders of selected samples were analyzed by Activation Laboratories, Ltd., by thermal ionization mass spectrometry using standard procedures. Depleted mantle model ages were calculated assuming linear isotopic growth for depleted mantle reservoir from $\varepsilon_{Nd}(t) = 0$ @ 4.55 Ga to $\varepsilon_{Nd}(0) = +10$ (or ^{143}Nd/^{144}Nd = 0.51315) at present, with ^{147}Sm/^{144}Nd = 0.2137 (Chen and Jahn, 1998). Present-day values of CHUR isotopic ratios and the decay constant for ^{147}Sm used in these calculations are as follows: ^{147}Sm/^{144}Nd = 0.1967, ^{143}Nd/^{144}Nd = 0.512638, and $\lambda_{147} = 6.54 \times 10^{-12}$ yr^{-1} (Rollinson, 1993).

RESULT

Whole-Rock Chemistry

Gneiss xenoliths found within the first- and second-generation gneisses range from gabbroic to dioritic in composition (47–54%

TABLE 2. (*Continued*)

Rock type	NDC Diorite Gneiss			NDC Mafics/Ultramafics					UHP Zone Gneiss		UHP Zone Granitic Gneiss	
Sample	FUZL-2	QLB-1	YZS-1	DB-117	RBZ-1	RBZ-2	RBZ-3	RBZ-4	SDH-1	YRZ-3	SZS-1	YRZ-1
SiO_2	54.3	47.5	49.1	46.2	46.7	46.1	45.7	42.9	64.8	63.8	78.0	76.7
TiO_2	1.47	1.70	1.77	0.89	1.21	1.08	0.99	0.13	0.77	0.82	0.11	0.17
Al_2O_3	16.3	17.6	17.5	10.8	13.4	13.0	14.8	3.18	15.5	15.3	11.7	12.4
Fe_2O_3	9.33	12.6	10.9	14.1	12.6	12.3	13.2	8.40	6.41	4.89	1.08	1.01
MnO	0.13	0.19	0.15	0.20	0.18	0.21	0.20	0.11	0.18	0.15	0.06	0.03
MgO	3.81	5.23	4.19	14.0	9.58	12.3	10.4	37.7	2.26	1.63	0.11	0.19
CaO	6.71	8.12	8.29	11.5	13.7	11.3	11.7	2.94	4.31	4.19	0.36	0.80
Na_2O	4.20	3.79	4.28	1.30	2.29	2.36	1.99	0.32	3.98	5.55	4.29	3.84
K_2O	2.21	2.32	2.03	0.61	0.12	0.54	0.36	0.04	1.90	1.58	3.99	4.22
P_2O_5	0.61	0.63	0.87	0.03	0.05	0.17	0.04	0.01	0.17	0.28	0.01	0.03
L.O.I.	0.45	0.49	0.62	0.65	0.34	0.92	0.19	4.27	0.32	2.42	0.13	0.39
Total	99.5	100.0	99.8	100.3	100.2	100.2	99.5	100.0	100.6	100.6	99.8	99.8
Li	26.1	40.1	26.4	3.61	6.34	6.25	5.32	–	13.5	7.02	2.39	7.53
Be	1.47	1.16	1.17	0.441	0.281	0.862	0.261	–	1.39	1.47	2.28	1.74
Sc	19.9	22.8	19.8	63.0	56.3	31.4	65.4	–	24.1	14.1	2.96	24.7
V	180	224	167	350	399	210	340	–	125	69.1	3.21	101
Cr	34.0	47.0	1.19	793	379	588	661	–	22.4	7.71	1.28	45.7
Co	43.6	44.4	35.3	99.3	136	63.4	102	–	45.1	64.6	134	79.7
Ni	31.3	30.6	3.30	237	96.8	20.2	16.4	–	11.5	5.06	0.979	22.2
Cu	20.0	29.7	24.2	65.1	71.8	73.8	64.5	–	13.0	16.8	1.34	13.9
Zn	96.4	115	111	89.3	15.8	15.6	13.9	–	81.3	69.2	51.3	94.0
Ga	22.0	22.2	21.6	13.2	1.61	1.64	1.77	–	17.4	18.0	18.5	19.4
Rb	62.4	66.0	91.5	14.0	6.79	12.8	13.5	–	45.6	31.3	94.0	29.0
Sr	613	996	998	77.3	115	610	211	–	199	321	29.8	614
Y	23.0	24.9	31.1	19.1	22.8	22.0	26.2	–	34.8	37.8	52.4	27.8
Zr	199	140	52.9	30.4	37.0	65.8	27.7	–	111	237	164	177
Nb	13.8	9.02	8.94	2.78	2.74	5.93	1.92	–	5.73	7.42	9.61	6.79
Sn	1.10	1.14	1.45	0.660	0.518	0.967	0.388	–	1.30	1.29	2.03	1.85
Cs	1.79	4.22	2.93	0.191	1.80	1.68	0.663	–	1.44	0.431	1.27	0.185
Ba	1400	1890	1010	142	115	379	116	–	503	829	905	969
La	51.3	43.3	39.4	6.73	5.11	7.59	0.075	–	15.8	32.3	34.9	26.7
Ce	103	95.7	86.6	19.1	12.4	18.8	0.344	–	32.8	64.7	72.6	53.6
Pr	12.4	12.8	11.7	2.73	1.97	2.59	0.112	–	4.17	8.20	9.12	7.04
Nd	49.8	55.5	51.4	12.0	9.43	12.3	1.11	–	17.7	34.7	33.6	28.7
Sm	8.36	9.92	9.63	2.83	2.46	3.23	1.29	–	3.88	6.98	7.59	5.96
Eu	2.77	3.69	3.26	0.776	0.809	0.945	0.617	–	1.14	2.16	0.950	1.64
Gd	6.86	7.54	7.66	2.73	2.47	2.97	2.12	–	3.79	6.09	6.76	4.97
Tb	0.897	1.04	1.11	0.503	0.501	0.528	0.496	–	0.773	1.02	1.28	0.838
Dy	4.64	5.28	5.94	3.15	3.27	3.25	3.46	–	5.37	6.35	8.22	5.01
Ho	0.857	0.962	1.15	0.725	0.762	0.714	0.852	–	1.29	1.40	1.91	1.05
Er	2.10	2.31	2.76	1.79	1.88	1.76	2.18	–	3.24	3.60	4.82	2.50
Tm	0.294	0.320	0.381	0.267	0.287	0.266	0.341	–	0.488	0.554	0.758	0.367
Yb	1.96	2.10	2.51	1.90	2.08	1.91	2.53	–	3.50	4.05	5.63	2.56
Lu	0.302	0.315	0.368	0.291	0.327	0.30	0.399	–	0.532	0.626	0.850	0.376
Hf	4.70	3.59	2.01	1.69	2.80	2.06	1.94	–	3.82	6.87	8.05	6.13
Ta	0.753	0.470	0.649	0.276	0.328	0.323	0.255	–	0.446	0.625	0.775	0.361
Pb	15.8	10.8	23.7	2.94	17.2	11.6	17.9	–	9.57	8.00	26.4	10.1
Th	3.92	1.67	2.85	0.118	<0.005	<0.005	<0.005	–	3.31	4.35	12.2	1.15
U	0.618	0.437	0.519	0.031	0.072	0.106	0.009	–	0.816	0.743	1.68	0.138

Note: NDC—Northern Dabie Complex; UHP—Ultra-high-pressure.

SiO_2) and are slightly to significantly more mafic than their host rocks. They are also dissimilar in composition to Northern Dabie Complex mafic/ultramafic rocks (see below).

First-generation gneisses range in SiO_2 from 58% to 69% and include both low- and high-K_2O variants. Second-generation gneisses display a similar variation in major element geochemistry, with compositions ranging from monzodioritic to granitic, with SiO_2 ranging from 58% to 75%, and they are slightly to strongly metaluminous. One granitic sample, QLB-3, is dissimilar to other second-generation gneisses both in geochemistry and appearance in hand sample and thin section. It is much more leucocratic than other second-generation gneisses but displays a clear gneissic texture that distinguishes it from the Northern Dabie Complex granites. In the field it crosscuts the second-generation gneisses. Excluding this sample from the set of second-generation gneisses makes their geochemical range much smaller, with SiO_2 ranging from 58% to 65%; the most felsic is a tonalite with the lowest K_2O. First- and second-generation gneisses are indistinguishable based on major element geochemistry alone as shown by Harker diagrams (Bryant, 2002). However, both groups of gneisses are usually much less felsic than Northern Dabie Complex granites.

Major element geochemistry of the Baimajian and Zhuboyuan Northern Dabie Complex granites reveal them both to be high-K granites with SiO_2 contents of 73%, marginally peraluminous, and with very similar major element compositions (Table 2).

The two varieties of ultra-high-pressure zone gneisses have distinctly different major element compositions. The ultra-high-pressure zone common gneisses have relatively low-K_2O tonalitic compositions while the ultra-high-pressure zone granitic gneisses are granitic and more felsic than the common gneisses.

Trace-element compositions (Table 2) of Northern Dabie Complex samples, excluding the mafic/ultramafic group, show a characteristic arc signature with a relative depletion of high field strength elements and enrichment of large ion lithophile elements in first- and second-generation gneisses (Fig. 4, A and B), granites (Fig. 4D), and to a lesser extent, diorite gneisses (Fig. 4C), consistent with previous studies (Zhai et al., 1994; Wang et al., 1996; Zhai and Cong, 1996; Zhang et al., 2000). Likewise, trace element patterns of the ultra-high-pressure zone granitic gneisses and to a lesser extent ultra-high-pressure zone common gneisses show an arc signature (Fig. 4E). Most ultra-high-pressure zone and Northern Dabie Complex samples plot within volcanic arc fields on Pearce diagrams (see Bryant, 2002). Mafic/ultramafic Northern Dabie Complex samples, however, do not exhibit this arc affinity (Fig. 4F). In summary, Northern Dabie Complex orthogneisses (Fig. 4, A–C) and granites (Fig. 4D) have island arc-like trace element signatures similar to those of gneisses in the Dabie ultra-high-pressure central zone (Fig. 4E and Zhai and Cong, 1996).

First- and second-generation gneisses and diorite gneisses are not readily distinguishable based on rare earth element (REE) patterns. Overall, gneisses are light REE (LREE)-enriched, with chondrite-normalized LREE ~70–220 and heavy REE (HREE) ~3–40 (Fig. 5, A–C). The Northern Dabie Complex granites exhibit negative Eu anomalies, setting them apart from Northern Dabie Complex gneisses that commonly show either a slight or no Eu anomaly at all (Fig. 5D). The two ultra-high-pressure zone common gneisses both lack Eu anomalies, but sample SDH-1 has lower LREE concentrations than sample YRZ-3 (Fig. 5E). The two ultra-high-pressure zone granitic gneisses are also dissimilar with SZS-1, having a negative Eu anomaly and an enrichment of HREEs, while YRZ-1 has no Eu anomaly and a depletion of HREEs (Fig. 5E). REE compositions do not readily distinguish ultra-high-pressure zone gneisses from first- or second-generation Northern Dabie Complex gneisses. As expected, Northern Dabie Complex mafic/ultramafic samples have REE patterns that are distinctly different from those of Northern Dabie Complex gneisses and granites (Fig. 5F) with relatively high HREE and low LREE concentrations, except

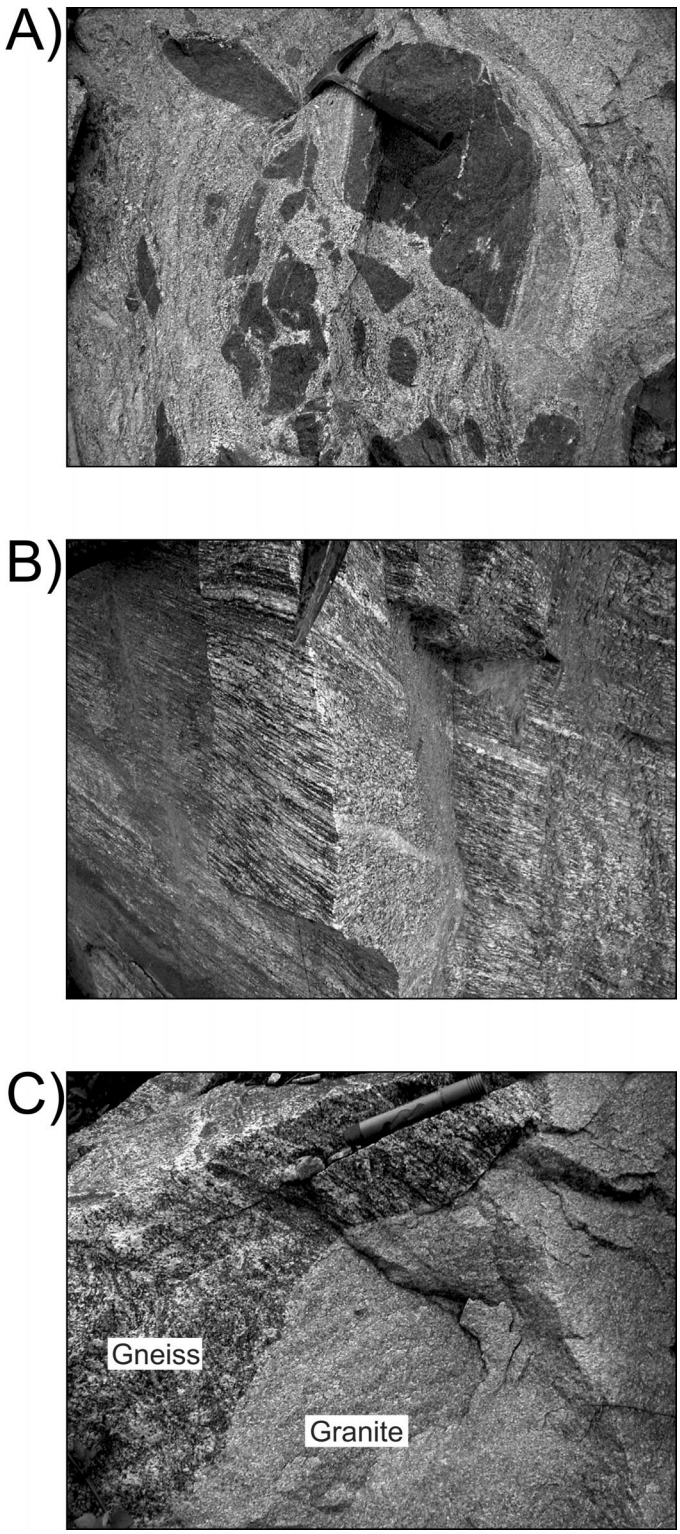

Figure 3. Field photographs of Northern Dabie Complex orthogneisses and granite. (A) First-generation gneiss enclosing diorite xenoliths. Location is Qilibai, 5 km west of Luotian, near core of Luotian dome. (B) Sample LTS-2, second-generation gneiss showing lineations, near Lutushishan (see Daogong et al., 2000). (C) Sample BMJ-3, first-generation gneiss in contact with Cretaceous Baimajian granite.

RBZ-3, which has very low LREE concentrations.

Zircon and Monazite Zoning and Geochronology

Most zircons from all samples are subhedral and show very little distinct internal zoning in backscattered electron images but strong zoning in cathodoluminescence images (see Table 3 for an explanation of monazite and zircon zoning terminology).

Northern Dabie Complex First-Generation Gneisses

Cathodoluminescence images reveal different dominant types of zoning within each of the three first-generation samples. LTS-1 zircons usually show concentric euhedral zoning or conformable core relationships (Fig. 6A). Zircons from QLB-2 (not shown) have mostly concentric euhedral zoning, but about one-third of them have modified zoning with featureless anhedral zones and only a few grains appear to have post-magmatic rims. Most of the WW-3 zircons, however, have concentric euhedral or modified zoning with post-magmatic rims that appear bright white in cathodoluminescence (Fig. 6B).

Many WW-3 analyses are slightly discordant, making their ^{206}Pb-^{238}U ages slightly younger than those from LTS-1 and QLB-2 (Table 4). Assuming the latter two samples to be representative of first-generation gneisses, the cumulative probability plot of ^{206}Pb-^{238}U ages yields a peak with a weighted mean age of 749 ± 18 Ma (n = 13, MSWD = 0.53; Fig. 7A) (mean square of weighted deviates) and a concordia age of 747 ± 14 Ma (n = 6, MSWD = 0.12; Fig. 7B) that we interpret to represent the crystallization age of the protoliths. These ages correspond to analysis spots from the inner and outer portions of individual zircon grains and agree well with Neoproterozoic ages previously reported by Hacker et al. (1998), Rowley et al. (1997), Xue et al. (1997), Wu et al. (2001), and Xie et al. (2001). The five highest-precision discordant analyses of WW-3 define a discordia line (Fig. 7C) with an upper intercept age of 781 +77/–65 Ma and a lower intercept age of 101 +110/–91 Ma (MSWD = 0.32). The upper intercept age agrees well with the ca. 750-Ma protolith age of first-generation gneisses LTS-1 and QLB-2 (Fig. 7, A and B). The lower intercept age may represent the timing of intrusion of the protolith of second-generation gneiss WW-4 (weighted mean ^{206}Pb-^{238}U age of 125 ± 5; n = 10, MSWD = 0.7), which may have initiated fluid activity (evident as centimeter- to meter-wide epidote-rich veins surrounded by

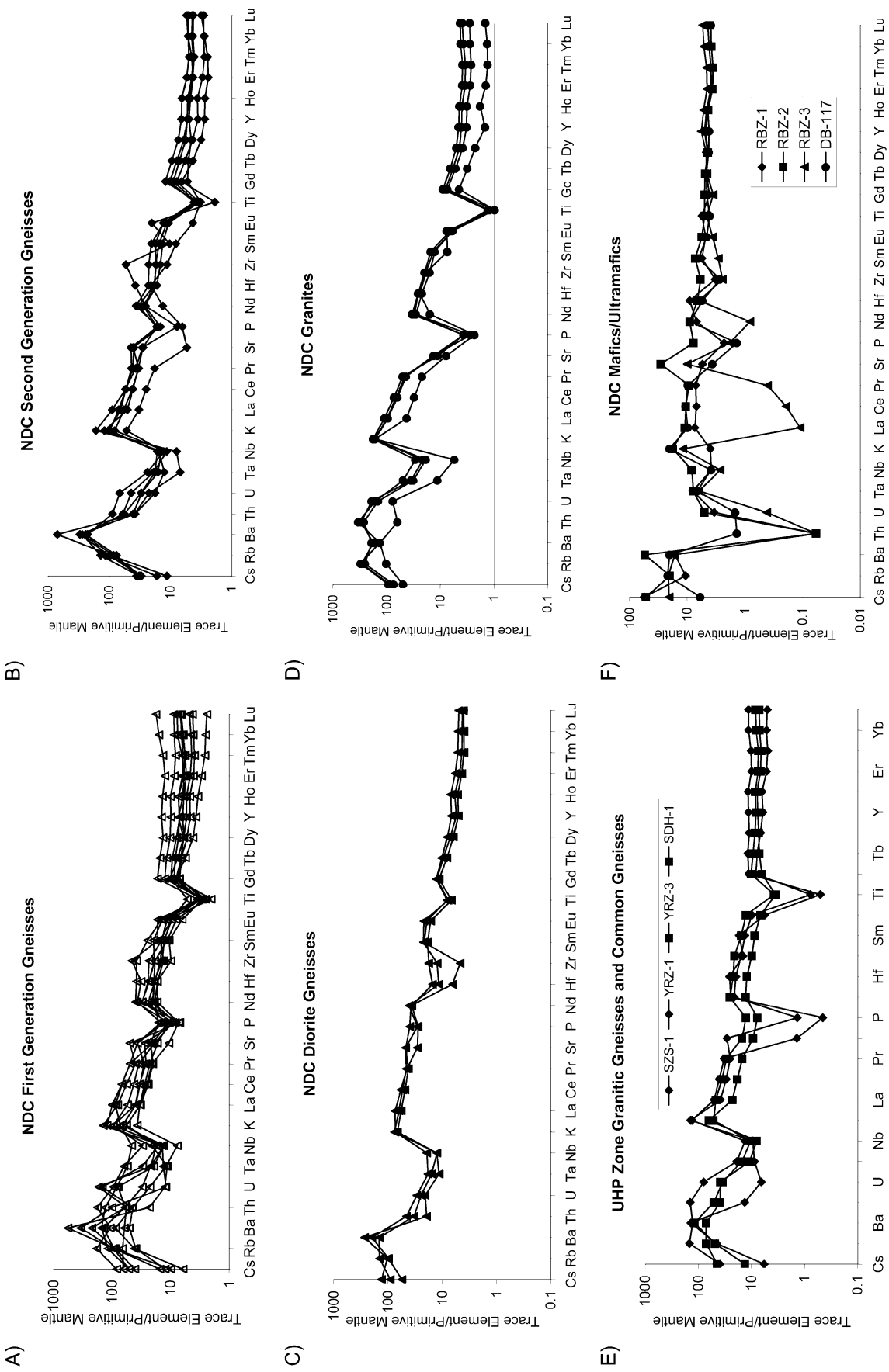

Figure 4. Trace element diagrams. (A) Northern Dabie Complex (NDC) first-generation gneiss samples; (B) NDC second-generation gneiss samples; (C) NDC diorite gneiss samples; (D) NDC granite samples; (E) ultra-high-pressure zone granitic gneiss (diamonds) and common gneiss (squares) samples; (F) NDC mafic/ultramafic samples.

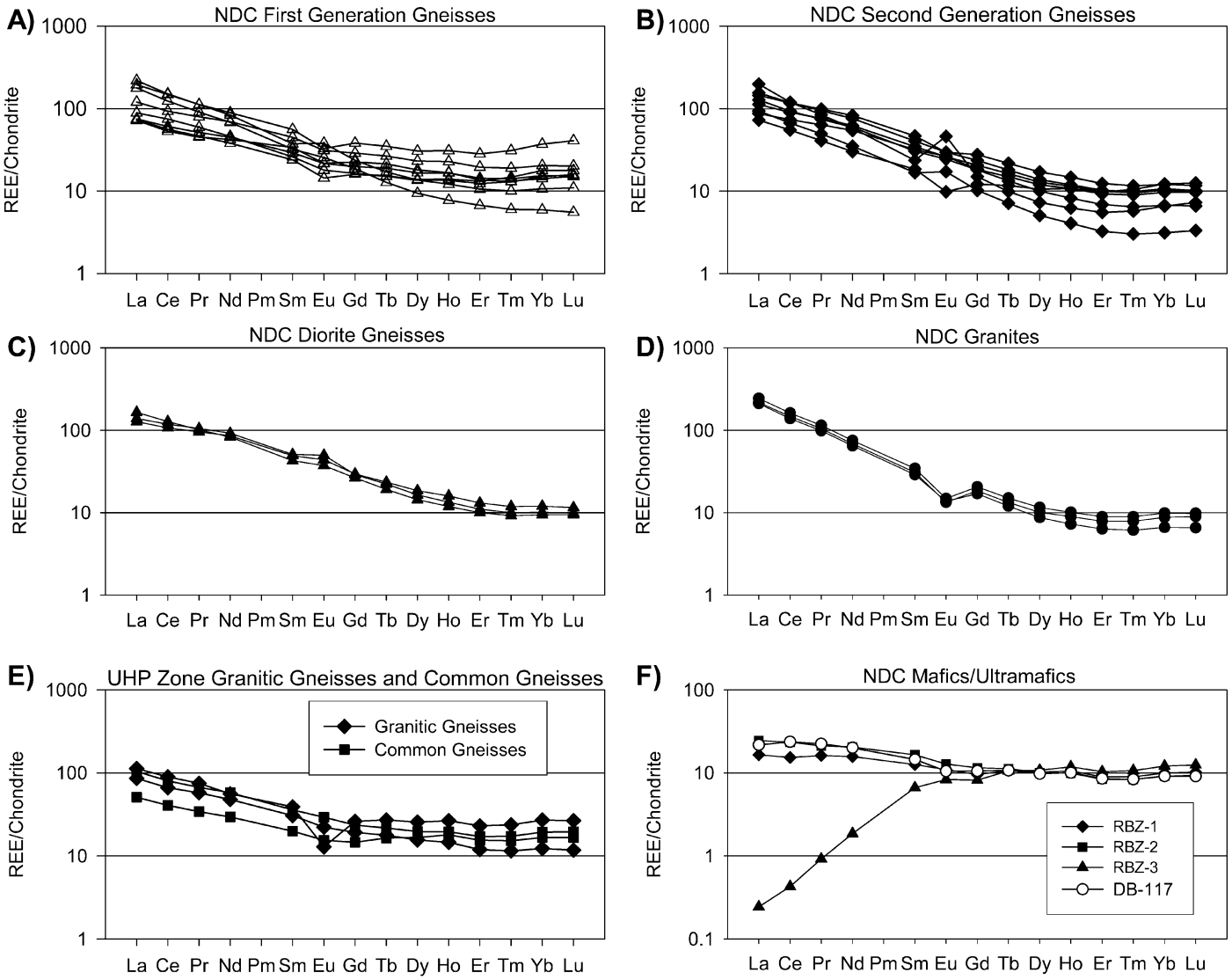

Figure 5. REE diagrams. (A) Northern Dabie Complex (NDC) first-generation gneiss samples; (B) NDC second-generation gneiss samples; (C) NDC diorite gneiss samples; (D) NDC granite samples; (E) ultra-high-pressure (UHP) zone granitic gneiss (diamonds) and common gneiss (squares) samples; (F) NDC mafic/ultramafic samples.

alteration haloes) and associated Pb loss from zircons in the adjacent rocks represented by WW-3. One concordant analysis of a metamorphic rim yields an age of 211 ± 11 Ma (Table 4). We obtained no ages younger than ca. 211 Ma, similar to findings by Chen et al. (2000).

Northern Dabie Complex Second-Generation Gneisses

About 80% of zircons from Northern Dabie Complex second-generation gneisses show concentric euhedral zoning in cathodoluminescence images (Fig. 6C) with the remaining grains displaying apparent inherited cores (Fig. 6D), modified zoning, or post-magmatic rims. These zircons yield a distinctly different set of age populations from the first-generation gneisses. All data points are concordant and yield two major groups of zircon ^{206}Pb-^{238}U dates with weighted means of 127 ± 4 (n = 16, MSWD = 0.57) and 271 ± 5 Ma (n = 2, MSWD = 0.051) (Fig. 8A). The Cretaceous age is similar to those obtained by Hacker et al. (1998) for Northern Dabie Complex gneisses and is found in whole zircon grains (analyses from both interior and exterior portions of a grain) and rims. The Permian age can be found as both cores and rims and is similar to a single ^{206}Pb-^{238}U zircon age of 280 ± 17 Ma found in the ultra-high-pressure zone granitic gneisses (see below). Two smaller modes give ages more similar to those of the first-generation gneisses at 606 ± 30 Ma (cores, n = 2, MSWD = 0.64) and 775 ± 37 Ma (cores and rims, n = 4, MSWD = 0.95). In addition, one significantly older zircon core yields a ^{207}Pb-^{206}Pb age of 2039 ± 95 Ma.

Northern Dabie Complex Diorite Gneiss

Zircons from Northern Dabie Complex diorite gneiss QLB-1, which occurs as a ~0.3-m diameter xenolith in first-generation gneiss at the Qilibai locality, generally have concentric euhedral zoning or modified zoning in cathodoluminescence images and often display a post-magmatic rim that is too small for analysis, much like those seen in sample WW-3. They yield two major groups of concordant ^{206}Pb-^{238}U dates (Fig. 8B). The largest

TABLE 3. ZONING TYPES

1. *Concentric euhedral zoning (CEZ):* Commonly finely oscillatory; magmatic, or much less commonly fluid phase, growth: external morphology often doubly terminated euhedral crystals.
2. *Sector zoning (SZ):* Differing zoning patterns occurring in distinct sectors with sharp boundaries. Caused by relatively rapid magmatic (possibly fluid) growth.
3. *Conformable cores (CC):* A clearly defined, subhedral to euhedral unzoned center of a grain with outer margin parallel to surrounding zoning.
4. *Modified zoning (MZ):* Secondary features that may significantly alter or reset U-Pb ratios. Can form during magmatic or fluid-related growth, metamorphism, or post-metamorphic metasomatism.
   a. Euhedral oscillatory zones truncated by unzoned, featureless zones that do not form a regular rim.
   b. Grains that are featureless and unzoned.
   c. Grains with heavily convoluted zoning.
5. *Apparent inherited cores (AIC):* A zoned or unzoned distinct core that is nonconformable with respect to surrounding zones. Often the unconformity is a resorption or abrasion surface where the core is inherited and the rim represents a new stage of growth.
6. *Fracturing (FR):* A secondary feature formed by either externally induced breakage or volume change related to radiation damage; can cause alteration of U-Pb ratios in the vicinity of the fracture.
7. *Post-magmatic rims (PMR):* Secondary growth of thin (usually <10 m), incomplete zones around earlier formed magmatic or fluid growth zones.

Note: Terminology used in the interpretation of internal zircon and monazite morphologies revealed by cathodoluminescence and backscattered electron images. After Mapes (2002).

of these age groups has a weighted mean of 770 ± 26 Ma (n = 6, MSWD = 0.59), and the smaller 953 ± 59 Ma (n = 5, MSWD = 0.63), both of which are representative of whole zircon grains. The latter group includes two discordant ages represented by ^{207}Pb-^{206}Pb ages of 1088 and 1034 Ma.

Northern Dabie Complex Granites

Zircons from the Baimajian Northern Dabie Complex granite often show concentric euhedral zoning in cathodoluminescence (Fig. 6F). Approximately one-third of the grains, however, have apparent inherited cores (Fig. 6E), while a few grains have modified zoning and lack distinct internal zoning patterns. This granite yields some zircons that, based on zoning (no apparent inherited cores) and multiple spot analyses within grains, are entirely Cretaceous in age, with ^{206}Pb-^{238}U ages that are mostly concordant and that range from ~108 to ca. 128 Ma with a weighted mean of 117 ± 11 Ma (n = 4, MSWD = 7.2) (Fig. 8D), similar to numerous previous studies (e.g., Zhang et al., 2002). Another group of zircons from the granite seem to be entirely Neoproterozoic in age, yielding a second large cluster of ^{206}Pb-^{238}U zircon ages with a weighted mean of 720 ± 65 Ma (n = 4, MSWD = 1.4) (Fig. 8D). A third cluster of ages representing zircon cores consists of one concordant ^{206}Pb-^{238}U and four discordant ^{207}Pb-^{206}Pb ages centered ~1941 ± 92 Ma (n = 5, MSWD = 1.8), similar to the single Proterozoic age of the second-generation gneiss. A discordia line defined by all analyses, except the ca. 720 Ma cluster (and grain #17 spot 2, which has a higher proportion of common Pb), has a lower intercept age of 112 ± 9 Ma and upper intercept age of 1941 +38/-39 Ma (n = 9, MSWD = 1.9) (Fig. 8C). The lower intercept is consistent with the concordant Cretaceous ^{206}Pb-^{238}U ages and is interpreted to represent the age of Pb loss from the older zircon cores.

The Cretaceous zircon ^{206}Pb-^{238}U ages agree with the weighted mean monazite ^{208}Pb- ^{232}Th age for the Baimajian granite of 117 ± 1 Ma (n = 15, MSWD = 2.0) (Fig. 8E, Table 5). Monazites from this sample occur primarily along grain boundaries with a few included or nearly included in biotite grains. The monazites are anhedral and show either modified zoning, especially featureless or unzoned, or sector zoning with two to three featureless zones (Fig. 6H). These grains never exhibit concentric euhedral zoning or definite core-rim relationships like many zircons in this study. All ages agree well with the Rb-Sr age of 112 ± 6 Ma reported for the Baimajian granite by Xu et al. (1994).

Ultra-High-Pressure Zone Granitic Gneisses

Zircons of the ultra-high-pressure zone granitic gneisses show two distinct types of zoning in cathodoluminescence, concentric euhedral zoning, and a heavily convoluted modified zoning associated with numerous inclusions (Fig. 6G). A post-magmatic rim commonly surrounds both types. Zircons from the ultra-high-pressure zone granitic gneisses generally yield concordant ages and have a weighted mean ^{206}Pb-^{238}U age of 698 ± 47 Ma (n = 6, MSWD = 1.3; Fig. 8F), similar to previously mentioned ages found in Northern Dabie Complex samples. However, the granitic gneisses also yield dates of 226 ± 8 Ma (n = 4, MSWD = 0.89) from grains with modified zoning and from post-magmatic rims. This age is consistent with previous dates of ultra-high-pressure zone rocks obtained by Ayers et al. (2002), H. Zhang et al. (2001), Hacker et al. (2000), and Li et al. (2000), among others. Another poorly defined peak occurs at 325 ± 110 Ma (n = 2, MSWD = 1.2).

Sm-Nd Analysis

Table 6 and Figure 9 summarize the results of the Sm-Nd isotopic analyses and calculations. Initial ε_{Nd} values span a wide range from −25.3 to −3.7, consistent with the range of −22.9 to + 3.2 for Northern Dabie Complex samples calculated for t = 760 Ma reported by Ma et al. (2000). The values of initial ε_{Nd} = −25.3 at the time of granite crystallization and T_{DM} = 2.3 Ga for Baimajian granite agree well with mean values of −24.4 and 2.2 Ga reported by Zhang et al. (2002) and the mean values of −21.2 and 2.05 Ga for the Zhuboyuan granite (Chen et al., 2002). Samples BMJ-1, a Northern Dabie Complex granite, and WW-4, a second-generation gneiss, have similar model ages at 2.25 and 2.32 Ga, respectively. Samples QLB-1, a Northern Dabie Complex diorite gneiss, and WW-3, a first-genation Northern Dabie Complex gneiss, also have similar depleted mantle model ages, 1.75 and 1.85 Ga, respectively. Sample QLB-2, another first-generation Northern Dabie Complex gneiss, yields an anomalously old model age at 3.56 Ga but has an unusually high ^{147}Sm/^{144}Nd ratio, indicating some fractionation event in its history. If we assume a ^{147}Sm/^{144}Nd ratio equal to that of sample WW-3 (0.1258), a typical crustal value, from the time of the fractionation of the sample from the depleted mantle until 677 Ma (the mean concordant zircon age from QLB-2 used to represent a time of a Sm/Nd fractionation event), the depleted mantle model age would be 2.10 Ga (two-stage model age), much closer to model ages of the other Northern Dabie Complex samples.

DISCUSSION

No mineralogical evidence was found in the samples analyzed here to support the hypothesis that the Northern Dabie Complex experienced ultra-high-pressure metamorphism. A limited electron microprobe survey showed no minerals or mineral compositions suggestive of a metamorphic grade exceeding amphibolite facies; mineral analyses are presented by Bryant (2002).

Constraints of Trace Element Geochemistry on Petrogenesis

The arc signature of the Northern Dabie Complex gneisses and granites has historically

TABLE 4. U/Pb ZIRCON GEOCHRONOLOGY DATA

Grain no.	Spot no.	Spot area[†]	Zoning type[‡]	Age (Ma) $^{206}Pb/^{238}U$	1σ	$^{207}Pb/^{235}U$	1σ	$^{207}Pb/^{206}Pb$	1σ	Pb Cor.[§]	% Rad. ^{206}Pb	$^{207}Pb^*/^{206}Pb^*$		$^{207}Pb^*/^{235}U$		$^{206}Pb^*/^{238}U$		ρ[#]
NDC Granite																		
Sample BMJ-1																		
1	1	core	AIH	114	2.7	116	13	156	268	204	99	0.049	(6)	0.12	(1)	0.0178	(4)	0.38
3	1	int	?	128	2.7	136	17	284	298	208	98	0.052	(7)	0.14	(2)	0.0200	(4)	0.35
7	1	core	AIH	731	30	754	30	825	50	204	100	0.067	(2)	1.10	(6)	0.120	(5)	0.92
7	2	rim	AIH	691	55	703	64	741	184	204	98	0.064	(6)	1.0	(1)	0.113	(9)	0.73
10	2	core	AIH	134	6.5	281	58	1805	375	208	95	0.11	(2)	0.32	(8)	0.021	(1)	0.70
11	1	ext	CEZ	108	4.2	112	14	185	277	208	97	0.045	(7)	0.12	(2)	0.017	(1)	0.49
13	1	core	AIH	1412	41	1603	40	1865	56	204	99	0.114	(4)	3.9	(2)	0.245	(8)	0.79
13	2	rim	AIH	1927	40	1927	25	1929	25	204	99	0.118	(2)	5.7	(2)	0.348	(8)	0.88
15	1	core	AIH	1487	74	1641	61	1844	86	204	98	0.113	(5)	4.0	(3)	0.26	(1)	0.77
15	2	core	AIH	1638	37	1814	33	2023	41	204	99	0.125	(3)	5.0	(2)	0.289	(7)	0.81
16	1	core	MZ, PMR	658	38	640	171	575	735	204	95	0.059	(2)	0.9	(3)	0.108	(7)	0.45
16	2	core	MZ, PMR	750	28	660	96	363	408	204	96	0.054	(1)	0.9	(2)	0.123	(5)	0.50
17	1	core	AIH	116	1.8	114	15	78	303	204	98	0.048	(6)	0.12	(2)	0.0182	(3)	0.48
17	2	core	AIH	178	9.0	141	91	–	–	204	92	0.039	(3)	0.1	(1)	0.028	(1)	0.57
Second-Generation Gneiss																		
Sample BMJ-3																		
5	1	core	CC	133	16	187	75	939	817	208	94	0.084	(2)	0.20	(9)	0.021	(2)	0.48
6	1	core	AIH	140	14	102	60	–	–	208	92	0.053	(2	0.11	(7)	0.022	(2)	0.38
6	2	core	AIH	127	13	107	83	–	–	208	91	0.066	(3)	0.11	(9)	0.020	(2)	0.41
6	3	rim	AIH	129	7.1	129	29	130	542	208	95	0.047	(2	0.14	(3)	0.020	(1)	0.34
13	1	core	AIH, MZ	227	34	100	224	–	–	208	83	0.021	(5)	0.1	(2)	0.036	(5)	0.29
13	2	rim	AIH, MZ	128	13	117	53	–	–	208	93	0.078	(2)	0.12	(6)	0.020	(2)	0.43
29	1	core	AIH	136	11	169	79	655	1018	208	91	0.025	(4)	0.18	(9)	0.021	(2)	0.48
Sample QLB-3																		
2	1	core	AIH	539	85	507	211	367	1069	204	93	0.054	(3)	0.6	(3)	0.09	(1)	0.47
2	2	rim	AIH	735	40	763	29	846	34	204	100	0.067	(1)	1.12	(6)	0.121	(7)	0.96
16	1	ext	CEZ	849	59	841	49	819	80	204	99	0.066	(3)	1.3	(1)	0.14	(1)	0.89
17	1	int	CEZ	799	46	805	39	822	65	204	100	0.067	(2)	1.21	(9)	0.132	(8)	0.90
Sample WW-4																		
1	1	int	CEZ	125	11	108	62	–	–	208	87	0.041	(2)	0.11	(7)	0.020	(2)	0.35
2	1	core	AIH	120	7.7	117	35	40	720	208	93	0.028	(2)	0.12	(4)	0.019	(1)	0.38
2	2	rim	AIH	132	12	114	47	–	–	208	94	0.05	(2)	0.12	(5)	0.021	(2)	0.45
5	1	int	CEZ,MZ	118	6.7	95	34	–	–	208	96	0.047	(8)	0.10	(4)	0.018	(1)	0.40
5	2	ext	CEZ,MZ	141	8.1	136	43	40	746	208	95	0.044	(2)	0.14	(5)	0.022	(1)	0.51
7	1	core	AIH	271	7.1	282	10	381	59	204	99	0.054	(1)	0.32	(1)	0.043	(1)	0.77
9	1	core	AIH, MZ	609	16	628	13	699	32	204	99	0.063	(1)	0.86	(2)	0.099	(3)	0.85
9	2	rim	AIH, MZ	123	9.8	78	47	–	–	208	92	0.058	(1)	0.08	(5)	0.019	(2)	0.40
10	1	int	CEZ	124	6.2	153	55	638	771	208	94	0.045	(2)	0.16	(6)	0.019	(1)	0.59
13	1	core	AIH	122	7.4	125	55	178	1028	208	92	0.014	(2)	0.13	(6)	0.019	(1)	0.51
13	2	rim	AIH	127	8.1	106	48	–	–	208	91	0.044	(2)	0.11	(5)	0.020	(1)	0.44
14	1	core	AIH	1971	195	2004	104	2039	47	204	99	0.126	(3)	6.2	(7)	0.36	(4)	0.97
18	1	core	AIH,MZ	770	27	785	21	827	23	204	100	0.067	(1)	1.17	(5)	0.127	(5)	0.96
18	2	rim	AIH,MZ	130	13	129	52	104	953	208	92	0.031	(3)	0.14	(6)	0.020	(2)	0.41
19	1	ext	MZ	277	27	273	59	243	486	208	95	0.064	(1)	0.31	(8)	0.044	(4)	0.52
First-Generation NDC Gneiss																		
Sample LTS-1																		
3	1	int	MZ	625	28	663	25	797	39	204	100	0.066	(1)	0.92	(5)	0.102	(5)	0.93
4	1	core	AIH	853	71	818	62	721	117	204	99	0.063	(3)	1.2	(1)	0.14	(1)	0.87
4	2	rim	AIH	661	69	547	152	98	762	204	95	0.048	(2)	0.7	(3)	0.11	(1)	0.48
12	1	core	CC	744	49	720	44	646	97	204	99	0.061	(3)	1.03	(9)	0.12	(1)	0.84
18	1	core	AIH,MZ	724	63	706	66	650	188	204	99	0.061	(5)	1.0	(1)	0.12	(1)	0.74
27	1	core	AIH,MZ	769	89	849	95	1063	257	204	98	0.075	(1)	1.3	(2)	0.13	(2)	0.64
Sample QLB-2																		
1	2	rim	AIH	752	32	620	145	163	681	204	98	0.049	(1)	0.8	(3)	0.12	(1)	0.51
3	1	core	AIH	613	15	643	12	752	13	204	100	0.064	(4)	0.88	(2)	0.100	(3)	0.97
3	2	rim	AIH	731	47	733	39	737	65	204	99	0.064	(2)	1.06	(8)	0.12	(1)	0.91
4	1	int	?	822	102	835	246	869	791	204	94	0.068	(3)	1.3	(6)	0.14	(2)	0.51
8	1	int	CEZ	730	44	750	40	812	70	204	100	0.066	(2)	1.09	(8)	0.12	(1)	0.90
10	1	int	MZ	444	25	298	271	–	–	204	89	0.03	(4)	0.3	(4)	0.071	(4)	0.54
13	1	int	CEZ	741	31	727	41	683	119	204	98	0.062	(3)	1.05	(8)	0.12	(1)	0.73
15	1	int	MZ	739	33	719	82	656	307	204	97	0.061	(9)	1.0	(2)	0.12	(1)	0.47
16	1	int	?	828	70	816	165	786	554	204	95	0.07	(2)	1.2	(4)	0.14	(1)	0.47
Sample WW-3																		
3	1	?	MZ,PMR	377	18	390	33	468	176	204	98	0.056	(4)	0.47	(5)	0.060	(3)	0.66
4	1	core	MZ,PMR	704	77	679	88	598	277	204	97	0.06	(8)	1.0	(2)	0.12	(1)	0.69
5	1	core	MZ,PMR	547	42	560	89	612	390	204	97	0.06	(1)	0.7	(2)	0.09	(1)	0.50
6	1	core	AIH	400	12	436	22	631	115	204	98	0.061	(3)	0.54	(3)	0.064	(2)	0.54
6	2	rim	AIH	268	13	192	24	–	–	208	96	0.051	(5)	0.21	(3)	0.042	(2)	0.45
7	1	core	MZ,PMR	541	40	592	41	793	97	204	99	0.066	(3)	0.79	(7)	0.09	(1)	0.86
10	1	core	MZ,PMR	513	43	644	65	1136	169	204	99	0.078	(7)	0.9	(1)	0.08	(1)	0.80

(*continued*)

TABLE 4. (*continued*)

Grain no.	Spot no.	Spot area†	Zoning type‡	Age (Ma) $^{206}Pb/^{238}U$	1σ	$^{207}Pb/^{235}U$	1σ	$^{207}Pb/^{206}Pb$	1σ	Pb Cor.§	% Rad. ^{206}Pb	$^{207}Pb^*/^{206}Pb^*$		$^{207}Pb^*/^{235}U$		$^{206}Pb^*/^{238}U$		ρ#
11	1	core	CC,PMR	658	24	679	21	751	33	204	100	0.064	(1)	0.95	(4)	0.107	(4)	0.93
13	1	core	CC,PMR	383	14	425	77	658	450	204	78	0.06	(1)	0.5	(1)	0.061	(2)	0.41
13	2	rim	CC,PMR	612	40	619	39	643	97	204	99	0.061	(3)	0.84	(7)	0.10	(1)	0.84
13	3	core	CC,PMR	592	32	630	32	772	56	204	99	0.065	(2)	0.86	(6)	0.10	(1)	0.93
16	1	core	AIH	674	63	665	116	636	439	204	95	0.06	(1)	0.9	(2)	0.11	(1)	0.53
17	1	core	CC,PMR	702	34	669	39	561	123	204	98	0.059	(3)	0.93	(7)	0.11	(1)	0.71
17	2	rim	CC,PMR	682	57	761	55	1002	133	204	100	0.073	(5)	1.1	(1)	0.11	(1)	0.77
17	3	rim	CC,PMR	655	41	678	39	758	82	204	99	0.065	(3)	0.95	(7)	0.11	(1)	0.87
18	1	core	AIH	334	14	382	17	684	66	204	99	0.062	(2)	0.46	(2)	0.053	(2)	0.82
18	2	rim	AIH	211	11	203	26	108	297	208	97	0.056	(7)	0.22	(3)	0.033	(2)	0.50
NDC Diorite Gneiss																		
Sample QLB-1																		
3	1	int	?	756	26	728	34	642	111	204	99	0.061	(3)	1.05	(7)	0.124	(5)	0.63
5	1	int	MZ	727	38	664	46	456	141	204	99	0.056	(4)	0.92	(9)	0.119	(7)	0.76
5	2	ext	MZ	1011	58	935	39	761	37	204	100	0.065	(1)	1.5	(1)	0.17	(1)	0.96
6	1	int	MZ	791	26	794	30	804	90	204	99	0.066	(3)	1.19	(7)	0.131	(5)	0.62
7	1	core	CC,FR	758	46	727	44	632	108	204	99	0.061	(3)	1.05	(9)	0.125	(8)	0.80
8	1	core	AIH	466	40	588	67	1088	230	204	100	0.076	(9)	0.8	(1)	0.075	(7)	0.65
9	1	int	?	978	90	940	135	851	370	204	96	0.07	(1)	1.5	(3)	0.16	(2)	0.61
10	1	int	?	620	75	717	91	1034	238	204	97	0.074	(9)	1.0	(2)	0.10	(1)	0.75
11	1	int	MZ	914	40	882	48	802	133	204	98	0.066	(4)	1.4	(1)	0.15	(1)	0.64
15	1	int	MZ	813	56	809	54	800	148	204	98	0.066	(5)	1.2	(1)	0.13	(1)	0.68
17	1	core	MZ,PMR	778	29	779	22	782	18	204	100	0.065	(6)	1.15	(5)	0.128	(5)	0.98
UHP Zone Granitic Gneiss																		
Sample SZS-1																		
5	1	core	MZ,FR,P	699	32	711	28	748	42	204	100	0.064	(1)	1.01	(6)	0.115	(6)	0.94
5	2	rim	MZ,FR,P	220	6.8	220	7.8	219	47	208	99	0.05	(1)	0.24	(1)	0.035	(1)	0.86
9	1	core	CC,MZ,P	764	54	762	40	758	51	204	100	0.064	(2)	1.12	(8)	0.126	(9)	0.95
9	2	rim	CC,MZ,P	228	8.0	232	7.6	272	29	208	100	0.053	(8)	0.26	(1)	0.036	(1)	0.94
11	1	int	MZ	235	7.9	223	7.6	97	34	208	99	0.053	(7)	0.25	(1)	0.037	(1)	0.93
19	1	core	MZ,PMR	280	8.6	207	8.3	–	–	208	97	0.052	(1)	0.23	(1)	0.044	(1)	0.78
Sample SZS††																		
1	1	core	AIH	935	127	899	116	811	243	204	98	0.066	(8)	1.4	(3)	0.16	(2)	0.80
6	1	core	CC	742	52	702	87	575	310	204	97	0.059	(8)	1.0	(2)	0.122	(9)	0.57
6	2	core	CC	906	64	801	72	519	227	204	98	0.058	(6)	1.2	(2)	0.15	(1)	0.60
40	1	int	MZ	647	34	584	60	343	253	204	97	0.053	(6)	0.8	(1)	0.106	(6)	0.58
42	1	int	MZ	667	37	674	39	699	96	204	99	0.063	(3)	0.94	(8)	0.109	(6)	0.83
42	2	ext	MZ	746	43	661	148	378	637	204	96	0.054	(2)	0.9	(3)	0.123	(8)	0.44
56	1	int	MZ	690	55	480	154	–	–	204	91	0.039	(1)	0.6	(2)	0.113	(9)	0.36
Sample YRZ††																		
1	1	int	MZ	202	31	201	30	188	216	204	100	0.05	(5)	0.22	(4)	0.032	(5)	0.84
17	1	int	MZ	341	16	338	20	319	93	204	99	0.053	(2)	0.39	(3)	0.054	(3)	0.81
21	1	int	MZ	1150	211	1049	134	845	70	204	99	0.067	(2)	1.8	(4)	0.20	(4)	0.99
44	1	int	MZ	320	9.5	339	10	472	28	204	100	0.057	(7)	0.40	(1)	0.051	(2)	0.93

†Indicates analysis performed on core or rim except where a clear core-rim relationship was not defined, in which case interior or exterior area of the grain is indicated.
‡Abbreviations from Table 3.
§Pb correction method.
#Correlation coefficient between x and y on concordia diagram.
††Zircons not taken from same sample as that used for geochemical analysis.

been the key piece of evidence in support of the hypothesis that the Northern Dabie Complex was a magmatic arc during the collision of the Yangtze and Sino–Korean plates (Zhai et al., 1994; Zhai and Cong, 1996). However, this arc signature can also be found in the ultra-high-pressure gneiss samples, which were part of the subducted region of the Yangtze plate and therefore could not have been part of an arc complex on the overriding Sino–Korean plate. Like the ultra-high-pressure region, the arc signatures of rocks in the Northern Dabie Complex may have developed during subduction-related magmatism at an earlier time.

Geochronological Constraints on the Evolution of the Northern Dabie Complex

Table 7 summarizes the measured ages and our interpretations. Based on zircon growth zoning relationships and ages corresponding to peaks in the cumulative age probability curves, we assign protolith crystallization ages of 770 ± 26 Ma to the diorite gneisses and ca. 750 Ma to the first-generation gneisses, consistent with field evidence that diorite gneisses frequently occur as blocks within first-generation gneisses. The oldest zircon ages obtained in any of the samples, though, are ~1.9–2.0 Ga from inherited cores in Cretaceous rocks, the Northern Dabie Complex granites, and the second-generation gneisses, which also commonly yield inheritance ages of ca. 750 Ma as observed by Hacker et al. (1998). The geochronologic data from the Northern Dabie Complex gneisses and granites show that a significant portion of the Northern Dabie Complex existed long before the Cretaceous and therefore that the Northern Dabie Complex did not form almost entirely by Cretaceous extensional magmatism.

The ~1.9–2.0 Ga ages obtained from inherited cores in Northern Dabie Complex granites and second-generation gneisses are consistent with previously reported ages from

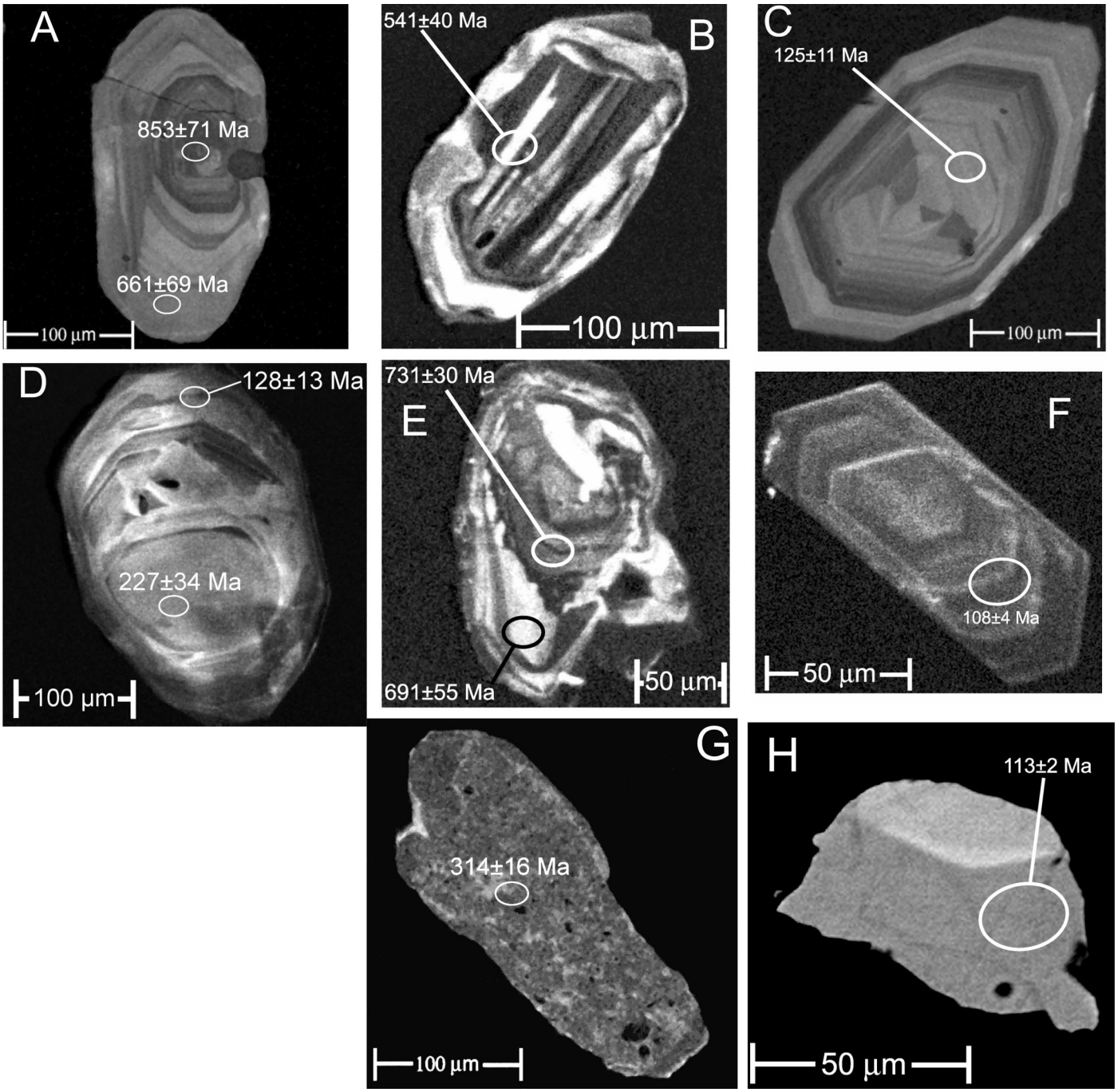

Figure 6. Images of dated grains. Ellipses mark ion microprobe analysis spots labeled with measured $^{208}Pb/^{232}Th$ ages for monazite and $^{206}Pb/^{238}U$ ages ($^{207}Pb/^{206}Pb$ ages if discordant) for zircon, with 1σ errors. (A) LTS1–04: cathodoluminescence image of zircon from first-generation Northern Dabie Complex gneiss sample LTS-1 showing concentric euhedral zoning. (B) WW3–07: Cathodoluminescence image of zircon from first-generation Northern Dabie Complex (NDC) gneiss sample WW-3 showing modified zoning and post-magmatic rim. (C) WW4b–01: Cathodoluminescence image of zircon from second-generation NDC gneiss sample WW-4 showing concentric euhedral zoning. (D) BMJ3–13: Cathodoluminescence image of zircon from second-generation gneiss BMJ3 with inherited core and concentric euhedral rim. (E) BMJ1–07: Cathodoluminescence image of zircon from NDC granite sample BMJ-1 showing modified zoning and an apparent inherited core. (F) BMJ1–11: Cathodoluminescence image of zircon from NDC granite sample BMJ-1 showing concentric euhedral zoning. (G) YRZ-31: Cathodoluminescence image of zircon from ultra-high-pressure zone sample YRZ-1 showing modified convoluted zoning with inclusions. (H) Backscattered electron image of monazite from NDC granite sample BMJ-1 showing sector zoning.

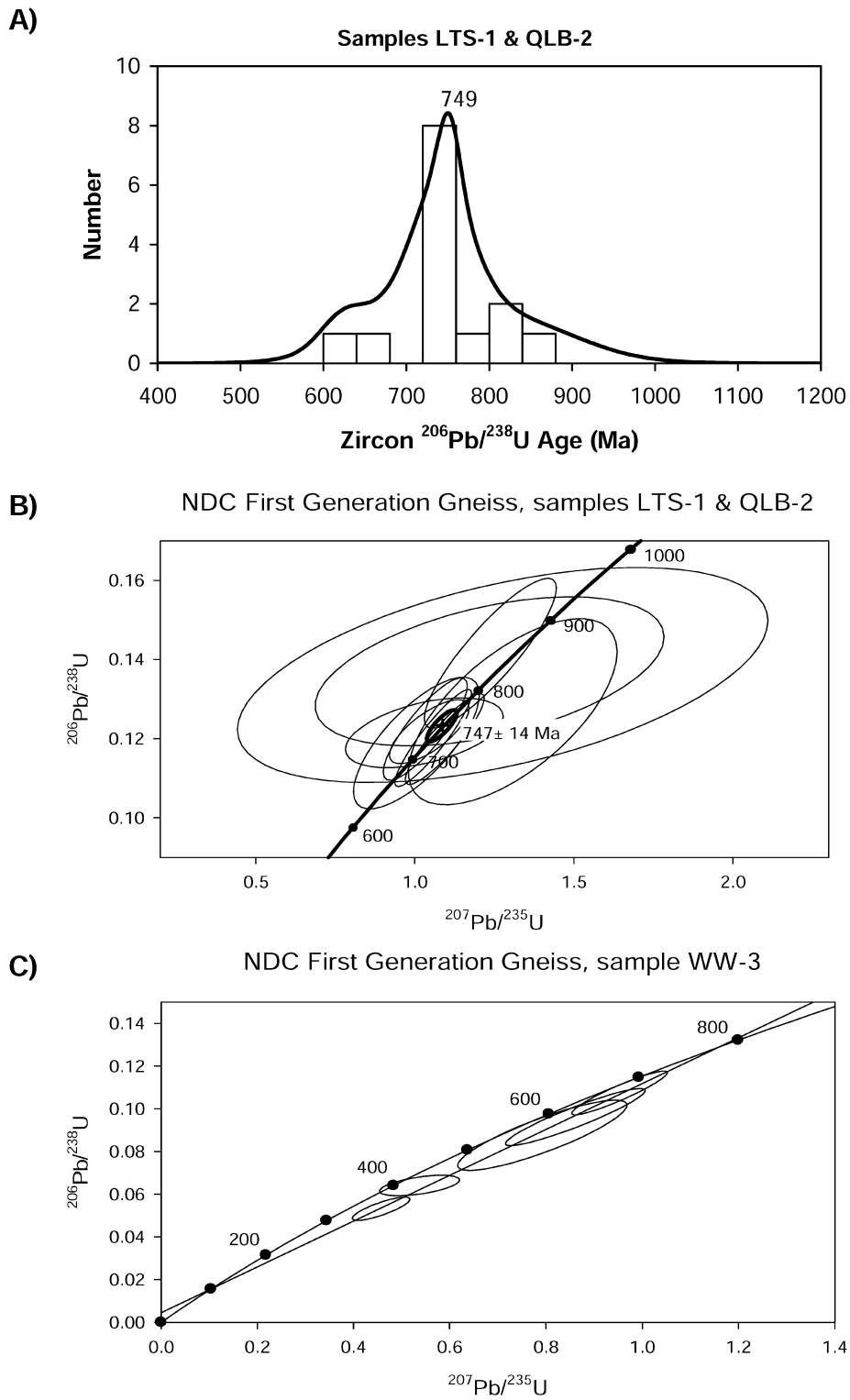

Figure 7. First-generation gneiss geochronologic data. Zircon ages on cumulative probability plots are $^{206}Pb/^{238}U$ ages. Peaks on cumulative probability plots are labeled with weighted mean of those analyses that define peak. Uncertainty ellipses on concordia diagrams are 68.3% confidence limits. (A) Cumulative probability plot and histogram of zircon U/Pb ages of first-generation Northern Dabie Complex (NDC) gneiss samples LTS-1 and QLB-2 ($^{207}Pb/^{206}Pb$ age used for QLB2–3–1; QLB-10–1 not included). (B) Concordia plot of concordant analyses from samples LTS-1 and QLB-2. Concordia Age = 747 ± 14 Ma (1σ, decay-constant errors included), MSWD of concordance = 0.117, Probability of concordance = 0.73. (C) Concordia diagram showing discordia defined by discordant analyses from sample WW-3. Intercepts at 101 +110/−91 Ma and 781 +77/−65 Ma, MSWD = 0.32.

the Yangtze craton, including ~1.9 Ga zircon ages related to intrusion of granites into Archean basement in the Kongling area ~150 km south of the Qinling-Dabie orogen (Qiu et al., 2000), and an upper concordia intercept age of zircon cores from the ultra-high-pressure zone at 1921 ± 22 Ma (Ayers et al., 2002; Marayuma et al., 1998). Jian et al. (1999) reported a significantly older Pb-Pb zircon age of 2456 ± 7 Ma from one intermediate granulite sample from the core of the Luotian dome near Luotian in the southwestern Northern Dabie Complex (Fig. 1). However, our samples QLB-1 and QLB-2, collected at Qilibai near the core of the Luotian dome, yielded no ages >1088 Ma. In contrast, basement rocks in the southern Sino–Korean craton yield U-Pb zircon magmatic ages of 2.51–2.84 Ga (Kroner et al., 1988). The next oldest age obtained for the Northern Dabie Complex samples we analyzed, ca. 950 Ma, is found only in the Northern Dabie Complex diorite gneiss xenoliths and may be a result of zircon growth during the final stages of the Jinningian orogeny, a ca. 1.0 Ga intensive tectonothermal and magmatic event that affected the northern margin of the Yangtze craton during the assembly of Rodinia.

All Northern Dabie Complex sample types have significant peaks in their cumulative age probability plots between 720 and 775 Ma (Figs. 7 and 8). Ages of 700–800 Ma can be found in every sample analyzed, including ultra-high-pressure zone samples. These ages make up ~40% of all analyses and are the dominant age groups for both the Northern Dabie Complex diorite and first-generation gneisses. This age range is particularly significant because it is the characteristic zircon age range for rocks of the Yangtze Craton (Rowley et al., 1997; Hacker et al., 1998, 2000; Zhang et al., 2002). The age overlap permits correlation of the Northern Dabie Complex directly with the Yangtze craton. The 700–800 Ma zircon ages are interpreted to represent the time of rifting that occurred along the northern margin of the Yangtze plate during the Sinian era (Rowley et al., 1997), causing the breakup

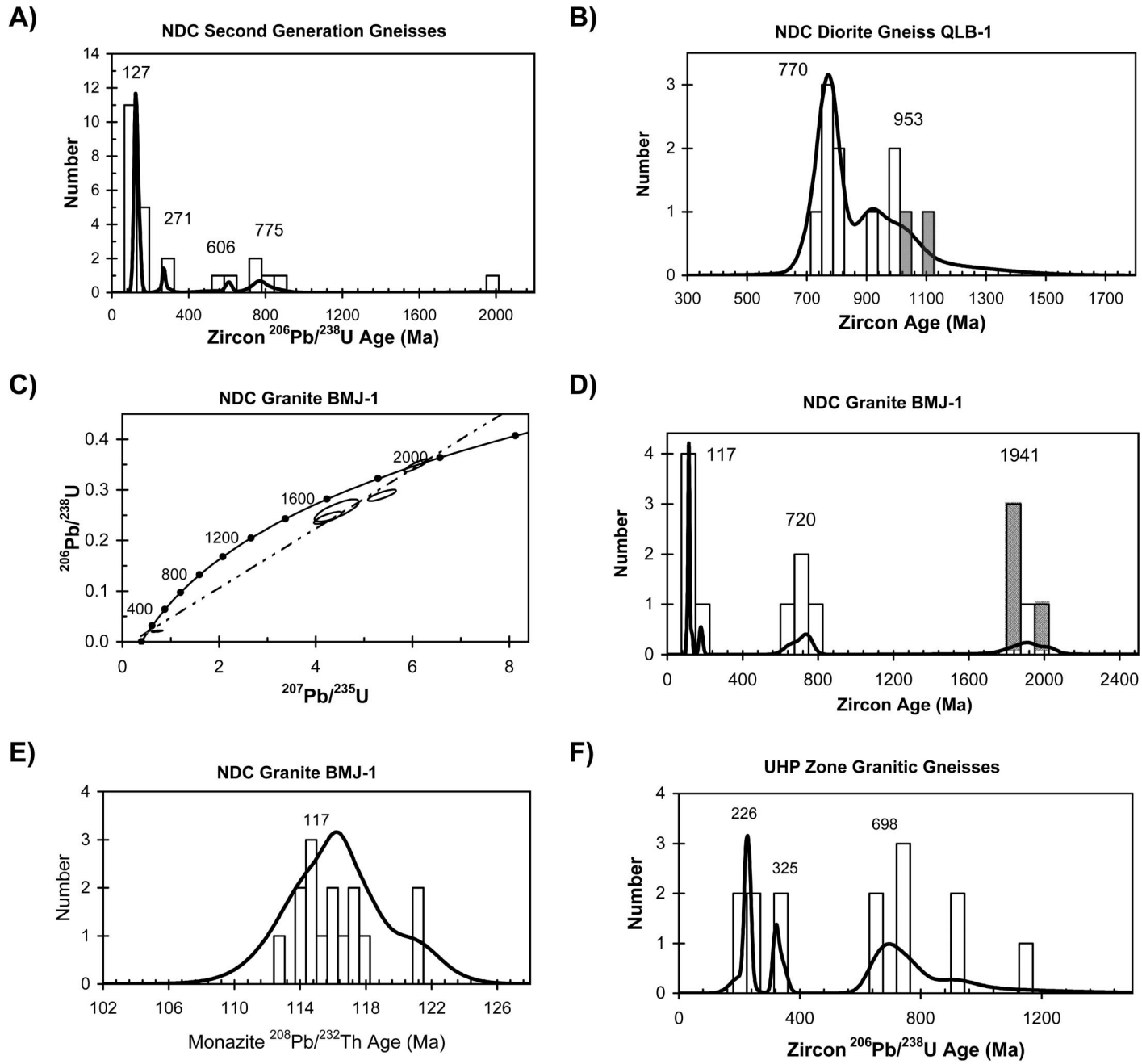

Figure 8. Geochronologic data for various lithologies. Zircon ages on cumulative probability plots are $^{206}Pb/^{238}U$ ages except for discordant analyses for which $^{207}Pb/^{206}Pb$ ages are plotted as shaded histogram bars. Peaks on cumulative probability plots defined by more than one analysis are labeled with weighted mean of those analyses that define peak. Uncertainty ellipses on concordia diagrams are 68.3% confidence limits. (A) Cumulative probability plot and histogram of zircon U/Pb ages of second-generation Northern Dabie Complex (NDC) gneiss samples. (B) Cumulative probability plot and histogram of zircon U/Pb ages of NDC diorite gneiss sample QLB-1. (C) Concordia plot of zircon analyses from Baimajian granite sample BMJ-1. Intercepts at 112 ± 9 Ma and 1941 +38/−39 Ma, MSWD = 1.9. (D) Cumulative probability plot and histogram of zircon U/Pb ages of Baimajian granite sample BMJ-1. (E) Cumulative probability plot and histogram of $^{232}Th/^{208}Pb$ monazite ages of Baimajian granite sample BMJ-1. (F) Concordia plot of zircon U/Pb data from ultra-high-pressure zone granitic gneiss samples.

of Rodinia (Li et al., 2002) and the crystallization of the protoliths of the diorite gneiss xenoliths and first-generation gneisses. These Proterozoic ages in the granites and second-generation gneisses represent an inherited component, suggesting that a thick section of crust, including possibly the magmatic source of these rocks, crystallized from crustal melts during rifting in the Sinian era (Table 7; Li et al., 2002). The four ca. 600 Ma ages obtained for the first- and second-generation Northern Dabie Complex gneisses are not clearly a distinctive age mode and may converge with the 700–800 Ma age group with additional analyses. It is also possible, however, that the ca.

TABLE 5. SAMPLE BMJ-1 MONAZITE GEOCHRONOLOGY DATA

Grain	Spot	Zoning type	$^{208}Pb/^{232}Th$ age (Ma)	1σ error (Ma)	$^{208}Pb/^{232}Th$	1σ	% Rad. ^{208}Pb
1	1	MZ,FR	120.9	1.4	0.00600	(7)	99.5
3	1	SZ,MZ	116.6	1.6	0.00579	(8)	99.7
3	2	SZ,MZ	117.4	3.0	0.0058	(2)	96.1
4	1	MZ	114.2	2.4	0.0057	(1)	99.7
5	1	MZ	116.1	2.5	0.0058	(1)	99.6
6	1	SZ,MZ	113.0	1.9	0.0056	(1)	99.4
7	1	MZ,FR	116.3	0.8	0.00577	(4)	99.6
8	1	MZ,FR	118.0	1.0	0.00585	(5)	97.6
11	1	MZ	121.3	1.9	0.00602	(9)	99.2
11	2	MZ	114.6	1.5	0.00568	(8)	99.0
15	2	SZ,MZ	114.1	2.8	0.0057	(1)	99.6
15	3	SZ,MZ	115.6	4.0	0.0057	(2)	99.4
16	1	MZ	114.9	2.0	0.0057	(1)	99.6
16	2	MZ	114.8	1.4	0.00570	(7)	99.2
18	1	MZ	117.0	1.4	0.00581	(7)	99.8

Note: Abbreviations from Table 3.

TABLE 6. SUMMARY OF Sm-Nd ISOTOPIC DATA AND CALCULATIONS FOR NDC SAMPLES

Rock type	Granite	Diorite Gneiss	1st Gen. Gneiss	1st Gen. Gneiss	2nd Gen. Gneiss
Sample	BMJ-1	QLB-1	QLB-2	WW-3	WW-4
Sm (ppm) (±0.5%)	5.42	9.25	6.47	8.67	5.49
Nd (ppm) (±0.5%)	36.3	51.6	24.1	41.6	32.3
$^{147}Sm/^{144}Nd$ (±0.5%)	0.0902	0.1083	0.162	0.1258	0.1025
$^{143}Nd/^{144}Nd$	0.51126	0.511939	0.511933	0.512082	0.511499
$\pm 2\sigma(\times 10^{-6})$	7	5	4	5	4
$\varepsilon_{Nd}(0)$	−26.8806	−13.6354	−13.7524	−10.8459	−22.2184
t (Ma)†	119	770	750	788	125
CHUR $^{143}Nd/^{144}Nd$ @ t	0.512485	0.511645	0.511671	0.511622	0.512477
$^{143}Nd/^{144}Nd$ @ t	0.511190	0.511392	0.511136	0.511432	0.511415
εNd(t)	−25.3	−4.94	−10.44	−3.71	−20.7
T_{DM} calculated (Ga)	2.32	1.75	3.56	1.85	2.25

† T—crystallization age.

600 Ma age represents some separate, previously unknown tectonothermal event.

All discordant analyses of first-generation gneiss sample WW-3 loosely define a discordia line with concordia intercepts at 781 +77/−65 Ma and 101 +110/−91 Ma (Fig. 7C). This is consistent with formation of first-generation gneisses protoliths during Sinian rifting followed by Pb loss during Cretaceous heating and extension.

If the Northern Dabie Complex was a magmatic arc in the Sino–Korean plate before and during the Triassic collision, late Paleozoic ages representing episodes of magmatism leading up to the collisional event should be found within the samples. However, no such ages were obtained for the samples we analyzed, permitting the preliminary conclusion that the Northern Dabie Complex was not an arc at the time of collision. Tsai et al. (2000) reached a similar conclusion in their study of the Jiaoziyan gabbro in the Northern Dabie Complex. The only late Paleozoic ages are within a small ca. 271 Ma age group of the second-generation Northern Dabie Complex gneisses and a single ^{206}Pb-^{238}U zircon rim age of 268 ± 13 Ma from first-generation gneiss sample WW-3. These ages could represent an unknown tectonothermal event that occurred before the Sino-Korean–Yangtze collision or the beginnings of the collision itself. However, the consensus is that the collision occurred in the Triassic, which is consistent with the 226 ± 8 Ma age obtained from the ultra-high-pressure zone granitic gneisses (Ayers et al., 2002; Hacker et al., 2000). We interpret this as the time of peak metamorphism of this area of the ultra-high-pressure zone. We obtained several similar ages from some Northern Dabie Complex samples, including a single zircon rim concordant age of 211 ± 11 Ma from first-generation Northern Dabie Complex gneiss sample WW-3 and an inheritance age of 227 ± 34 from second-generation gneiss sample BMJ-3 (Fig. 6D). These Triassic zircon ages may represent the time of peak metamorphism, but they are much rarer in the Northern Dabie Complex than in the central ultra-high-pressure zone, suggesting that the Northern Dabie Complex may not have experienced the same intensity of metamorphism as the ultra-high-pressure zone to the south.

In the Cretaceous, the entire Dabie orogen experienced crustal extension and related magmatism (Hacker et al., 2000). The second-generation gneisses intruded the Northern Dabie Complex at ca. 125 Ma and were subsequently deformed; intrusion of the Northern Dabie Complex granites followed at ca. 117 Ma.

Sm-Nd Constraints on Evolution of the Northern Dabie Complex

The low values of initial ε_{Nd} calculated for Northern Dabie Complex granite (−25.3) and second-generation gneisses (−20.7) argue against a significant mantle contribution to the magmas that crystallized to form the granite and second-generation gneiss protoliths (Table 6). Combined with the ancient inheritance demonstrated by zircon U-Pb results, low initial ε_{Nd} values suggest that Northern Dabie Complex granites and second-generation gneisses formed by partial melting of old (>1.5 Ga) crust. However, the large difference between their Cretaceous ε_{Nd} values suggests that partial melting of diorite gneiss and/or first-generation gneiss alone could not produce the Northern Dabie Complex granites and second-generation gneiss protoliths.

Northern Dabie Complex diorite gneiss QLB-1 (T_{DM} = 1.75 Ga) and first-generation gneiss WW-3 (T_{DM} = 1.85 Ga) (Table 6) have depleted mantle model ages much older than the magmatic crystallization ages of ca. 750 Ma recorded by zircons (Table 7), suggesting that their protoliths were derived by partial melting of continental crust at ca. 750 Ma during Sinian era rifting. Northern Dabie Complex granite BMJ-1 (2.32 Ga) and second-generation gneiss WW-4 (2.25 Ga) model ages fall within the range of 1.6–2.4 Ga reported for Cretaceous granites throughout the Dabie orogen (Zhang et al., 2002). These Paleoproterozoic model ages along with highly negative ε_{Nd} values (Table 6) show that Northern Dabie Complex gneiss protoliths and Northern Dabie Complex granite formed by partial melting of continental crust that formed long before Cretaceous extension, which argues against formation of the Northern Dabie Complex almost entirely by extensional magmatism during the Cretaceous (Hacker et al., 1998).

The interpretation that the Northern Dabie Complex is Yangtze crust agrees with recent interpretations based on Sr, Nd, and Pb isotopic data that the Northern Dabie Complex underlies the central Dabie ultra-high-pressure zone (Fig. 10) in the Yangtze craton and that partial melting of the Northern Dabie Complex or similar Yangtze non-ultra-high-pressure crustal rocks produced Cretaceous granites throughout the Dabie orogen (Zhang et al., 2002). Recent interpretations of seismic data by Schmid et al. (2001) showing the pres-

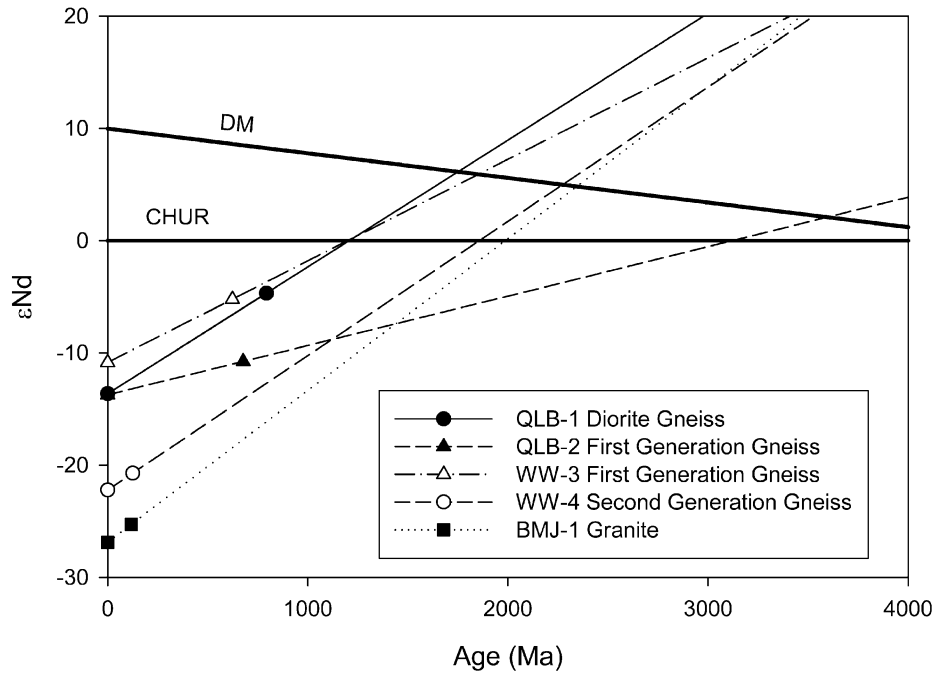

Figure 9. Plot of ε_{Nd} versus time for selected samples. Plotted points indicate present-day ($\varepsilon_{Nd}(0)$) and initial ($\varepsilon_{Nd}(t)$) values for each sample (from Table 6). Lines passing through these two points for each sample are extrapolated to where they intersect depleted mantle evolution line, which gives depleted mantle model age T_{DM} (depleted mantle model evolution from Chen and Jahn, 1998).

ence in the central Dabie of what may be Yangtze crust unaffected by ultra-high-pressure metamorphism beneath a thin cover of ultra-high-pressure rocks also support this interpretation.

Petrogenesis of Northern Dabie Complex Second Generation Gneisses and Granites

Large differences in $\varepsilon_{Nd}(t)$ values rule out the possibility that the Northern Dabie Complex granites ($\varepsilon_{Nd}(125)$ of BMJ-1 $=-25.2$) and second-generation gneiss protoliths ($\varepsilon_{Nd}(125)$ of WW-4 $=-20.7$) could have formed solely by partial melting of first-generation gneisses ($\varepsilon_{Nd}(125)$ of WW-3 $=-9.7$) or diorite gneisses ($\varepsilon_{Nd}(125)$ of QLB-1 $=-12.2$). Based on Nd and Sr isotope systematics, Ma et al. (2000) proposed that the Archean Kongling gneisses that crop out just south of the Dabie orogen extend beneath it and that early Cretaceous felsic gneisses in the Northern Dabie Complex (our second-generation gneisses, their group II gneisses) represent mixtures of Kongling gray gneiss + Neoproterozoic mantle-derived material. The description by Ma et al. (2000) of the Kongling gneisses (gray-banded orthogneiss with volcanic arc trace element signatures containing enclaves of foliated amphibolites) sounds remarkably similar to our observations of first-generation gneisses with diorite gneiss xenoliths in the Northern Dabie Complex; however, the Kongling gray gneisses are Archean and have much lower ε_{Nd} values ($\varepsilon_{Nd}(0)$ ~-40 to -45, Ma et al., 2000; -37 to -50, Gao et al., 1999). Based on Nd isotope compositions alone, we cannot rule out the possibility that second-generation gneiss protoliths represent mixtures of Kongling gray gneiss and first-generation or diorite gneiss. The absence of inherited Archean zircons is inconsistent with but does not rule out the possibility of a Kongling gneiss component, and the ca. 2 Ga zircons correspond to zircon ages from granites in the Kongling region (Qiu et al., 2000).

Like the second-generation gneiss protoliths, the Northern Dabie Complex granites may have formed by partial melting of ancient lower continental crust with highly negative ε_{Nd}, a conclusion reached by Chen et al. (2002) in their study of the Zhubuyuan granite. This source must have had significant feldspar in the residue to produce the Eu depletion in the REE patterns (Fig. 5D) and low Sr concentrations characteristic of the Northern Dabie Complex granites. Using Nd-Sr mixing calculations, Ma et al. (2000) showed that the Northern Dabie Complex granites (their group III) do not appear to have a significant Kongling gneiss component, but an intermediate granulite from the Northern Dabie Complex served as an appropriate end-member component. This interpretation is consistent with that of Gao et al. (1998) that intermediate granulites compose the lower crust of the Dabie orogen. These intermediate granulites could, if they contained hydrous phases such as biotite or hornblende, produce granitic magmas with compositions similar to those observed in the Baimajian and Zhubuyuan plutons. The interpretation that Northern Dabie Complex granites formed by partial melting of intermediate granulites in the lower crust is also consistent with the conclusions of Zhang et al. (2002) that Cretaceous granites in the Northern Dabie Complex and ultra-high-pressure/high pressure zones formed by partial melting of Northern Dabie Complex basement rocks and that the unradiogenic Pb isotope compositions of Cretaceous granites indicate U-depleted source rocks such as granulites.

Ma et al. (2000) proposed an alternative explanation: that the Cretaceous granites could have formed by partial melting of second-generation gneisses and subsequent fractional crystallization. This model seems plausible given their similar values of $\varepsilon_{Nd}(t)$ and that trace element compositions of Cretaceous granites are similar to but more evolved (higher incompatible and lower compatible element concentrations) than those of second-generation gneiss protoliths. The substantial difference in crystallization ages rules out the possibility that second-generation gneiss protoliths and then granites were derived from the same magmas at a given locality. For example, at Baimajia, second-generation gneiss BMJ-3 crystallized at 130.8 ± 4 Ma and granite BMJ-1 crystallized at 117 ± 11 Ma. In summary, the model we prefer involves extension and heating of the lower crust ca. 130 Ma (Ratschbacher et al., 2000); partial melting of Kongling basement mixed with first-generation and diorite gneisses to form second-generation gneiss protoliths, deformation of the second-generation gneisses, and partial melting of granulite basement or second-generation gneisses, followed by intrusion of granites into second-generation gneisses at ca. 117 Ma.

Tectonic Synthesis

While most Northern Dabie Complex samples have a typical arc trace element signature, the Northern Dabie Complex was not a magmatic arc immediately before the Triassic collision, as evidenced by the lack of late Paleozoic zircon ages in the Northern Dabie Complex samples. However, abundant Precambrian U-Pb zircon ages suggest that a sub-

TABLE 7. SUMMARY OF MEASURED AGES AND INTERPRETATIONS

Samples	Cretaceous		Permo-Triassic		Sinian Era		Minor age peaks	
	Age[†] (Ma)	Interpretation	Age (Ma)	Interpretation	Age (Ma)	Interpretation	Age (Ma)	Interpretation
NDC								
Granite (BMJ-1)	117 ± 11[‡] (monazite 117 ± 1)	Magmatic crystallization age			720 ± 65	Inherited grains crystallized during major crustal growth event associated with Sinian era rifting of Rodinia	1941 ± 42	Formation of Yangtze craton in Paleo-Proterozoic
2nd Gen. Gneisses (BMJ-3, QLB-3, WW-4)	127 ± 4	Crystallization of protolith	271 ± 13	Tectonothermal event associated with Yangtze/Sino-Korean collision?	775 ± 37	″	606 ± 30	?
1st Gen. Gneisses (LTS-1 and QLB-2)					747 ± 14	Crystallization of protolith during Sinian era rifting		
Diorite Gneiss (QLB-1)					770 ± 26	″	953 ± 59	Jinningian orogeny in neo-Proterozoic: assembly of Rodinia
UHP Zone								
Granitic Gneisses (SZS-1 and YRZ-1)			226 ± 8	Peak metamorphism in UHP zone	698 ± 47	″		

Note: Total # of analyses: zircon = 100, monazite = 15; UHP—Ultra-high-pressure.
[†]Ages are weighted average of measured zircon ages with 95% confidence limits unless otherwise stated.
[‡]Underlined age groups represent the mode of the age distribution for that sample.

stantial portion of the Northern Dabie Complex existed before the Triassic. Protoliths of the Northern Dabie Complex diorite gneiss xenoliths and Northern Dabie Complex first-generation gneisses crystallized at ca. 770 and 750 Ma, respectively. The 720–775 Ma zircon ages and ca. 2 Ga Sm-Nd crustal residence ages found in all Northern Dabie Complex gneiss and granite samples analyzed are similar to values measured for rocks from the central ultra-high-pressure and high-pressure zones that are accepted as part of the Yangtze plate but distinctly different from values obtained from the Sino–Korean plate, suggesting that the Northern Dabie Complex is part of the Yangtze plate (Hacker et al., 2000).

The recent discovery of eclogites and microdiamond-bearing eclogites in the northernmost Northern Dabie Complex has been used to suggest ultra-high-pressure metamorphism and deep continental subduction of the entire Northern Dabie Complex (Tsai and Liou, 2000; Xu et al., 2000, 2003; Liu et al., 2001). Geological observations, however, indicate that these eclogites and microdiamond-bearing eclogites are always separated from the underlying gneiss by a detachment fault (Suo et al., 2003). This, combined with the relative rarity of Triassic zircon U-Pb ages compared with the central ultra-high-pressure zone, and the absence of ultra-high-pressure assemblages in all but the northernmost Northern Dabie Complex even in mafic lithologies, suggests an alternative interpretation that the Northern Dabie Complex was not deeply subducted in the Triassic. This interpretation agrees with the conclusions of Zhang et al. (2002) and Schmid et al. (2001) that the ultra-high-pressure zone is presently a shallow crustal feature underlain by Yangtze rocks similar to the Northern Dabie Complex (Fig. 10). We interpret this tectonic configuration to result from thrusting of the ultra-high-pressure zone onto the Yangtze craton during exhumation (Fig. 10B; Wang et al., 2000). Emplacement of the ultra-high-pressure zone as a thrust sheet onto the Northern Dabie Complex with subsequent thermal relaxation would cause heating of the footwall to higher temperatures than in the hanging wall. This explains why geothermometers record higher temperatures in the Northern Dabie Complex (granulite grade) than in non-ultra-high-pressure lithologies in the central ultra-high-pressure zone (amphibolite grade). It is also consistent with the clockwise P-T trajectories of gneisses in the Northern Dabie Complex (Zheng et al., 2001) and their nearly isothermal decompression from ~12 to 8 kbar (Zhang et al., 1996). Mafic rocks just south of the Xiaotian–Mozitang fault that preserve evidence of ultra-high-pressure metamorphism may represent erosional remnants of the portion of the ultra-high-pressure slab that penetrated most deeply into the mantle and therefore experienced the highest pressures (Fig. 10). Unlike mafic lithologies, felsic gneisses in the ultra-high-pressure slab were completely retrogressed during exhumation. Gneisses in the Northern Dabie Complex formed during partial subduction (Fig. 10B) or during burial following thrust-stacking of the ultra-high-pressure slab onto the Northern Dabie Complex (Fig. 10C).

Slab detachment and subsequent upwelling of asthenosphere may have caused delamination of the crustal eclogite root (see Gao et al., 1998) and lithospheric mantle keel that was subsequently replaced (Fig. 10, B and C; Gao et al., 2002). Upwelling of hot asthenosphere through the gap opened by detachment of the sinking slab of oceanic lithosphere may have initiated post-collisional extension and doming in the Cretaceous (Fig. 10, C and D; Coulon et al., 2002). Heating caused partial melting of the Northern Dabie Complex basement (first-generation gneisses) to form second-generation gneiss protoliths ca. 125 Ma and Northern Dabie Complex granites around ca. 117 Ma. Doming caused erosion of the overlying ultra-high-pressure rock and exposure of the Northern Dabie Complex but preservation of ultra-high-pressure erosional remnants in the northernmost Northern Dabie Complex (Figs. 1 and 10E).

Since the Northern Dabie Complex is part of the Yangtze plate, the Sino-Korean–Yangtze suture must lie to the north of the Yangtze plate, possibly along the Xiaotian–Mozitang fault. Hacker et al. (1998, 2000) have used 700–800 Ma inherited zircon ages from granites of the North Huaiyang to argue that the Yangtze plate extends north of the Xiaotian–Mozitang fault. Alternatively, these inherited zircons and their host granites may have been derived from Yangtze crust lying beneath a north-dipping suture and the Sino–Korean craton. The tectonic configuration shown in Figure 10E and described above would account for the presence of Yangtze zircon ages in North Huaiyang granites formed by partial melting of Yangtze crust underlying the Sino–Korean craton. However, it is still possible that the suture lies to the north of the Xiaotian–Mozitang fault (Hacker et al., 2000).

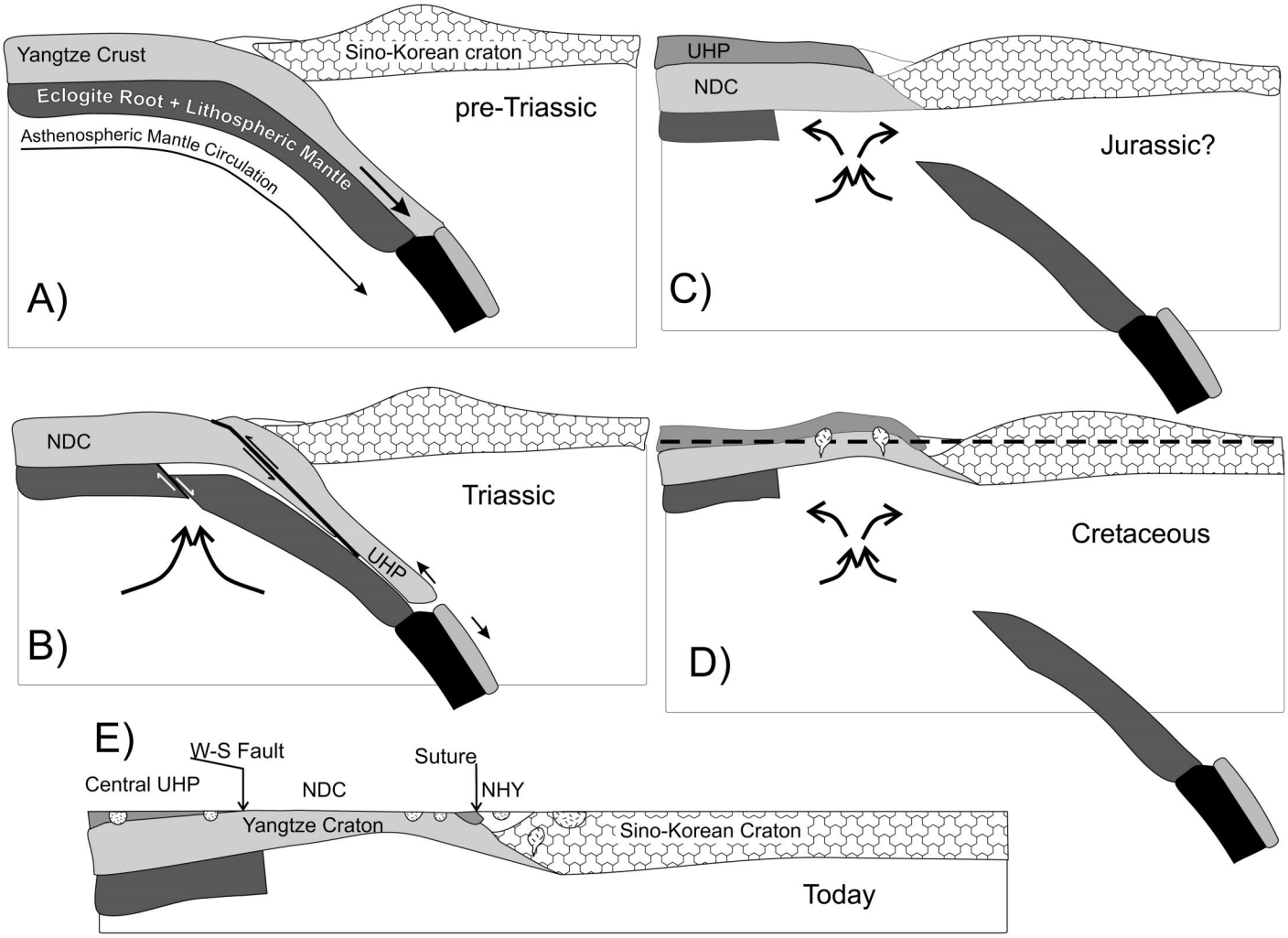

Figure 10. Schematic sequence of tectonic events. (A) Subduction of Yangtze continental lithosphere beneath Sino–Korean Craton and peak ultra-high-pressure (UHP) metamorphism in Triassic. (B) Detachment of oceanic lithosphere followed by delamination of Yangtze eclogitic lower crust and lithospheric mantle and exhumation of ultra-high-pressure slab. (C) Transport of ultra-high-pressure hanging wall along thrust fault and emplacement atop Northern Dabie Complex (NDC) footwall. Initiation of asthenospheric upwelling through gap opened by detachment of slab and lithospheric root. (D) Crustal thinning and extension causes melting of NDC lower crust in Cretaceous and emplacement of second-generation gneiss protoliths followed by NDC granites. (E) Erosion exposes NDC but leaves an intact UHP slab in central Dabie and ultra-high-pressure erosional remnant in northernmost NDC.

ACKNOWLEDGMENTS

This material is based upon work supported by the National Science Foundation under Grant Nos. EAR-0126020 and EAR-9873626 to Ayers and Natural Science Foundation of China grants to Shan Gao (Grant 40133020) and to Hongfei Zhang (Grant 49794043). Any opinions, finding, conclusions, or recommendations expressed in this material are those of the authors and do not necessarily reflect the views of the National Science Foundation. Support for geochemical analyses came from the Key Laboratory of Continental Dynamics, Northwest University. Thanks to Allen Patchen for help with the electron probe microanalyzer at the University of Tennessee, Knoxville, and Marty Grove and Kevin McKeegan for help with the ion microprobe at the University of California, Los Angeles (UCLA). The UCLA ion microprobe is partially subsidized by a grant from the National Science Foundation Instrumentation and Facilities Program. Thorough reviews by Ian Fitzsimons, Brad Hacker, and Associate Editor David Moecher helped to greatly improve the manuscript.

REFERENCES CITED

Ayers, J.C., Dunkle, S., Gao, S., and Miller, C.F., 2002, Constraints on timing of peak and retrograde metamorphism in the Dabie Shan Ultra-high-pressure Metamorphic Belt, east-central China, using U-Th-Pb dating of zircon and monazite: Chemical Geology, v. 186, p. 315–331.

Bryant, D.L., 2002, Geochemical, age, and isotopic constraints on the location of the Sino–Korean/Yangtze Suture and evolution of the Northern Dabie Complex [M.S. thesis]: Nashville, Tennessee, Vanderbilt University, 111 p.

Chen, J., and Jahn, B.-M., 1998, Crustal evolution of southeastern China: Nd and Sr isotopic evidence: Tectonophysics, v. 284, p. 101–133.

Chen, D., Deloule, E., Xia, Q., and Cheng, H., 2000, Preliminary U-Pb ion probe age determination of zircons from gneisses, Northern Dabie Terrain: Acta Petrologica Sinica, v. 16, p. 199–202.

Chen, B., Jahn, B.-M., and Wei, C., 2002, Petrogenesis of Mesozoic granitoids in the Dabie ultra-high-pressure complex, Central China: Trace element and Nd-Sr isotope evidence: Lithos, v. 60, p. 67–88.

Coulon, C., Megartsi, M., Fourcade, S., Maury, R.C., Bellon, H., LouniHacini, A., Cotten, J., Coutelle, A., and Hermitte, D., 2002, Post-collisional transition from calc-alkaline to alkaline volcanism during the Neogene in Oranie (Algeria): Magmatic expression of a slab breakoff: Lithos, v. 62, p. 87–110.

Daogong, C., Deloule, E., Qunke, X., and Hao, C., 2000, Preliminary U-Pb ion probe age determination of zircons from gneisses, Northern Dabie Terrain: Acta Petrologica Sinica, v. 16, p. 199–202.

Gao, S., Luo, T.-C., Zhang, B.-R., Zhang, H.-F., Han, Y.-W., Zhao, Z.-D., and Hu, Y.-K., 1998, Chemical composition of the continental crust as revealed by studies in East China: Geochimica et Cosmochimica Acta, v. 62, p. 1959–1975.

Gao, S., Ling, W., and Simon, K., 1999, Contrasting geochemical and Sm-Nd isotopic compositions of Archean metasediments from the Kongling high-grade terrain of the Yangtze craton: Evidence for cratonic evolution and redistribution of REE during crustal anatexis: Geochimica et Cosmochimica Acta, v. 63, p. 2071–2088.

Gao, S., Rudnick, R.L., Carlson, R.W., McDonough, W.F., and Liu, Y.S., 2002, Re-Os evidence for replacement of ancient mantle lithosphere beneath the North China craton: Earth and Planetary Science Letters, v. 198, p. 307–322.

Hacker, B.R., Wang, X., Eide, E.A., and Ratschbacher, L., 1996, The Qinling-Dabie ultra-high-pressure collisional orogen, *in* Yin, A., and Harrison, M., eds., Metamorphism and tectonics of high-pressure and ultra-high-pressure belts in the Dabie-Sulu region, China: New York, Cambridge University Press, p. 345–370.

Hacker, B.R., Ratschbacher, L., Webb, L., Ireland, T., Walker, D., and Shuwen, D., 1998, U/Pb zircon ages constrain the architecture of the ultra-high-pressure Qinling-Dabie Orogen, China: Earth and Planetary Science Letters, v. 161, p. 215–230.

Hacker, B.R., Ratschbacher, L., Webb, L., McWilliams, M.O., Ireland, T., Calvert, A., Dong, S., Wenk, H.-R., and Chateigner, C., 2000, Exhumation of Ultra-high-pressure continental crust in east central China: Late Triassic–Early Jurassic tectonic unroofing: Journal of Geophysical Research, v. 105, p. 13,339–13,364.

Jahn, B.-M., Wu, F., Lo, C.-H., and Tsai, C.-H., 1999, Crust-mantle interaction induced by deep subduction of the continental crust: Geochemical and Sr-Nd isotopic evidence from post-collisional mafic-ultramafic intrusions of the northern Dabie complex, central China: Chemical Geology, v. 157, p. 119–146.

Jian, P., Yang, W., and Zhang, Z., 1999, $^{207}Pb/^{206}Pb$ zircon dating of the Huangtuling hypersthene-garnet-biotite gneiss from the Dabie Mountains, Hubei Province, China: New evidence for early Precambrian evolution: Acta Geologica Sinica, v. 73, p. 78–83.

Kroner, A., Compston, V., Zhang, G., Guo, A., and Todt, W., 1988, Age and tectonic setting of late Archean greenstone-gneiss terrain in Henan Province, China, as revealed by single-grain zircon dating: Geology, v. 16, p. 211–215.

Li, S., Xiao, Y., Liou, D., Chen, Y., Ge, N., Zhang, Z., Sun, S.-s., Cong, B., Zhang, R., Hart, S.R., and Wang, S., 1993, Collision of the North China and Yangtse blocks and formation of coesite-bearing eclogites: Timing and processes: Chemical Geology, v. 109, p. 89–111.

Li, S., Jagoutz, E., Chen, Y., and Li, Q., 2000, Sm-Nd and Rb-Sr isotopic chronology and cooling history of the ultrahigh pressure metamorphic rocks and their country rocks at Shuanghe in the Dabie Mountains, central China: Geochimica et Cosmochimica Acta, v. 64, p. 1077–1093.

Li, Z.-X., Li, X.-H., Zhou, H., and Kinny, P.D., 2002, Grenvillian continental collision in south China: New SHRIMP U-Pb zircon results and implications for the configuration of Rodinia: Geology, v. 30, p. 163–166.

Liou, J.G., Zhang, R.Y., Ernst, W.G., Rumble, D., III, and Maruyama, S., 1998, High-pressure minerals from deeply subducted metamorphic rocks, *in* Hemley, R.J., ed., Ultrahigh-Pressure Mineralogy: Physics and Chemistry of the Earth's Deep Interior: Washington, D.C., The Mineralogical Society of America Reviews in Mineralogy, v. 37, p. 33–96.

Liu, Y., Xu, S., Li, S., Chen, G., Jiang, L., Zhou, C., and Wu, W., 2001, Distribution and metamorphic P-T condition of eclogites from the mafic-ultramafic belt in the northern Dabie Mountains: Acta Geologica Sinica, v. 75, p. 385–395 (in Chinese, with English Abstract).

Ludwig, K.R., 2000, Isoplot/Ex version 2.49: A geochronological toolkit for Microsoft Excel: Berkeley Geochronology Center Special Publication 1a, 53 p.

Ma, C., Ehlers, C., Xu, C., Li, Z., and Yang, K., 2000, The roots of the Dabieshan ultra-high-pressure metamorphic terrane: Constraints from geochemistry and Nd-Sr isotope systematics: Precambrian Research, v. 102, p. 279–301.

Mapes, R.W., 2002, Geochemistry and geochronology of Mid-Paleozoic granitic plutonism in the southern Appalachian piedmont terrane, North Carolina-South Carolina-Georgia [M.S. thesis]: Nashville, Tennessee, Vanderbilt University, 150 p.

Marayuma, S., Tabata, H., Nutman, A.P., Morikawa, T., and Liou, J.G., 1998, SHRIMP U-Pb geochronology of ultra-high-pressure metamorphic rocks of the Dabie Mountains, central China: Continental Dynamics, v. 3, p. 72–85.

Miller, C.F., Hatcher, R.D., Jr., Ayers, J.C., Coath, C.D., and Harrison, T.M., 2000, Age and zircon inheritance of eastern Blue Ridge plutons, southwestern North Carolina and northeastern Georgia, with implications for magma history and evolution of the southern Appalachian orogen: American Journal of Science, v. 300, p. 142–172.

Nelles Verlag, 1998, Central China: Munchen, Nelles Verlag GmbH, scale 1:1,500,000.

Paces, J.B., and Miller, J.D.J., 1993, Precise U-Pb ages of Duluth Complex and related mafic intrusions, northeastern Minnesota: Geochronological insights to physical, petrogenetic, paleomagnetic, and tectonomagmatic processes associated with the 1.1 Ga Midcontinent Rift System: Journal of Geophysical Research, v. 98, p. 13,997–14,013.

Qiu, Y.M., Gao, S., McNaughton, N.J., Groves, D.I., and Ling, W., 2000, First evidence of >3.2 Ga continental crust in the Yangtze craton of south China and its implications for Archean crustal evolution and Phanerozoic tectonics: Geology, v. 28, p. 11–14.

Quidelleur, X., Grove, M., Lovera, O.M., Harrison, T.M., Yin, A., and Ryerson, F.J., 1997, Thermal evolution and slip history of the Renbu Zedong Thrust, southeastern Tibet: Journal of Geophysical Research, v. 102, p. 2659–2679.

Ratschbacher, L., Hacker, B.R., and Wenk, H.-R., 2000, Exhumation of the ultra-high-pressure continental crust in east central China: Cretaceous and Cenozoic unroofing and the Tan-Lu fault: Journal of Geophysical Research, v. 105, p. 13,303–13,338.

Rollinson, H., 1993, Using geochemical data: Evaluation, presentation, and interpretation: Singapore, Longman Singapore Publishers Ltd., 352 p.

Rowley, D.B., Xue, F., Tucker, R.D., Peng, Z.X., Baker, J., and Davis, A., 1997, Ages of ultra-high-pressure metamorphism and protolith orthogneisses from the eastern Dabie Shan: U/Pb zircon geochronology: Earth and Planetary Science Letters, v. 151, p. 191–203.

Schmid, R., Ryberg, T., Ratschbacher, L., Schulze, A., Franze, L., and Oberhänsli, R., 2001, Crustal structure of the eastern Dabie Shan interpreted from deep reflection and shallow tomographic data: Tectonophysics, v. 333, p. 347–359.

Stacey, J.S., and Kramers, J.D., 1975, Approximation of terrestrial lead isotope evolution by a two-stage model: Earth and Planetary Science Letters, v. 26, p. 207–221.

Suo, S.T., Zhong, Z.Q., Zhou, H.W., and You, Z.D., 2003, Massive eclogites and their tectonic significance in Dabie-Sulu ultra-high-pressure metamorphic belt, East-Central China: Earth Sciences, v. 28, p. 111–120 (in Chinese, with English abstract).

Tsai, C.-H., and Liou, J.G., 2000, Eclogite-facies relics and inferred ultra-high-pressure metamorphism in the Northern Dabie Complex, central-eastern China: American Mineralogist, v. 85, p. 1–8.

Tsai, C.-H., Lo, C.-H., Liou, J.G., and Jahn, B.-M., 2000, Evidence against subduction-related magmatism for the Jiaoziyan Gabbro, northern Dabie Shan, China: Geology, v. 28, p. 943–946.

Wang, Q., Zhai, M., and Cong, B., 1996, Regional Geology, *in* Bolin, C., ed., Ultra-high-pressure metamorphic rocks in the Dabieshan-Sulu region of China: Boston, Kluwer Academic Publishers, p. 8–26.

Wang, C.-Y., Zeng, R.-S., Mooney, W.D., and Hacker, B.R., 2000, A crustal model of the ultra-high-pressure Dabie Shan orogenic belt, China, derived from deep seismic refraction profiling: Journal of Geophysical Research, v. 105, p. 10,857–10,869.

Wu, Y., Chen, D., Deloule, E., Xia, Q., Li, B., and Cheng, H., 2001, Zircon U-Pb ion probe ages of gneisses from the Northern Dabie Terrain and their geological implications: Geological Review, v. 47, p. 239–244.

Xie, Z., Chen, J.F., Zhang, X., Gao, T.S., Dai, S.Q., Zhou, T.X., and Li, H.M., 2001, Zircon U-Pb dating of gneiss from the Shizhue in North Dabie and its geologic implications: Acta Petrologica Sinica, v. 17, p. 139–144.

Xu, S., Okay, A.I., Shouyuan, J., Şengör, A.M.C., Wen, S., Yican, L., and Laili, J., 1992, Diamond from the Dabie Shan metamorphic rocks and its implication for tectonic setting: Science, v. 256, p. 80–82.

Xu, S., Liu, Y., Jiang, L., and Su, W., 1994, Tectonic regime and evolution of Dabie Mountains (in Chinese, with English abstract): Beijing, Science Press, 235 p.

Xu, S., Liu, Y., and Su, W., 2000, Discovery of the eclogite and its petrography in northern Dabie Mountains: Chinese Science Bulletin, v. 45, p. 273–278.

Xu, S., Liu, Y., Chen, G., Compagnoni, R., Rolfo, F., He, M., and Liu, H., 2003, New findings of microdiamonds in eclogites from Dabie-Sulu region in central-eastern China: Chinese Science Bulletin, v. 48, p. 988–994.

Xue, F., Rowley, D.B., Tucker, R.D., and Peng, Z.X., 1997, U-Pb zircon ages of granitoid rocks in the Northern Dabie Complex, Eastern Dabie Shan, China: Journal of Geology, v. 105, p. 744–753.

Zhai, M., and Cong, B., 1996, Major and trace element geochemistry of eclogites and related rocks, *in* Bolin, C., ed., Ultra-high-pressure metamorphic rocks in the Dabieshan-Sulu region of China: Boston, Kluwer Academic Publishers, p. 69–89.

Zhai, M., Bolin, C., Qi, Z., and Qingchen, W., 1994, The Northern Dabieshan Terrain: A possible Andean-type arc: International Geology Review, v. 36, p. 867–883.

Zhang, R.Y., Liou, J.G., and Tsai, C.H., 1996, Petrogenesis of a high-temperature metamorphic terrane; a new tectonic interpretation for the north Dabieshan, central China: Journal of Metamorphic Geology, v. 14, p. 319–333.

Zhang, H., Zhang, B., Zhong, Z., Gao, S., and Hu, S., 2000, Geochemistry of gneisses from Dabie Complex and Tongbai Complex in Qinling-Tongbai-Dabie Orogenic Belt: Implications for location of Yangtze-Sino–Korean Suture: Journal of China University of Geosciences, v. 11, p. 392–405.

Zhang, H., Zhong, Z., Gao, S., Zhang, B., and Li, H., 2001, U-Pb zircon age of the foliated garnet-bearing granites in western Dabie Mountains, central China: Chinese Science Bulletin, v. 46, p. 1657–1660.

Zhang, H., Gao, S., Zhong, Z., Zhang, B., Zhang, L., and Hu, S., 2002, Geochemical and Sr-Nd-Pb isotopic compositions of Cretaceous granitoids constraints on tectonic framework and crustal structure of the Dabieshan ultra-high-pressure metamorphic belt, China: Chemical Geology, v. 186, p. 281–299.

Zheng, Y.-F., Fu, B., Li, Y.-L., Wei, C.-S., and Zhou, J.-B., 2001, Oxygen isotope composition of granulites from Dabieshan in eastern China and its implications for geodynamics of Yangtze Plate subduction: Physics and Chemistry of the Earth (A), v. 26, p. 673–684.

Manuscript Received by the Society 19 May 2003
Revised Manuscript Received 15 September 2003
Manuscript Accepted 22 September 2003

Printed in the USA